Title: PRRT2 as an auxiliary regulator of Nav channel slow inactivation

Authors: Bin Lu[1,8*], Qi-Wu Xu[1,8], Jing Zhang[1,8], Xue-Mei Wu[1,2,8], Jun-Yan He[1,3,8], Guang Yang[1,3,6], Ke-Xian Li[4], Ling Zhuang[1,3,7], Yu-Xian Zhang[1], Zhi-Qi Xiong[1,2,3,5,9*]

Affiliations:

[1]Center for Excellence in Brain Science and Intelligence Technology (Institute of Neuroscience), Chinese Academy of Sciences, Shanghai 200031, China

[2]School of Life Science and Technology, ShanghaiTech University, Shanghai 201210, China

[3]University of Chinese Academy of Sciences, Beijing 100049, China

[4]Department of Neurology, Zhongshan Hospital, Fudan University, Shanghai 200032, China

[5]Shanghai Center for Brain Science and Brain-Inspired Intelligence Technology, Shanghai 201210, China

[6]Present address: Interdisciplinary Research Center on Biology and Chemistry, Shanghai Institute of Organic Chemistry, Chinese Academy of Sciences, Shanghai 201210, China

[7]Present address: Hainan Academy of Medical Sciences, Hainan Medical University, Hainan 571199, China

[8]These authors contributed equally: Bin Lu, Qi-Wu Xu, Jing Zhang, Xue-Mei Wu, Jun-Yan He.

[9]Lead contact

[*]Correspondence: lubin@ion.ac.cn (B.L.), xiongzhiqi@ion.ac.cn (Z-Q.X.)

Abstract

During sustained activity, voltage-gated sodium (Nav) channels enter a slow-inactivated state to limit cellular hyperexcitability. Disruption of this regulatory process has been implicated in skeletal, cardiac and neurological disorders. While the kinetics of this process are well characterized, its endogenous modulators remain unclear. Here, we identify Proline-Rich Transmembrane Protein 2 (PRRT2) as a native regulator of Nav channel slow inactivation. We show that PRRT2 facilitates the entry of Nav channels into slow-inactivated state and delays their recovery, a regulatory effect conserved from zebrafish to humans. PRRT2 forms molecular complexes with Nav channels both *in vitro* and *in vivo*. In the mouse cortex, PRRT2 deficiency impairs the slow inactivation of Nav channels in neuronal axons, leading to reduced cortical resilience in response to hyperexcitable challenges. Together, these findings establish PRRT2 as a physiological modulator of Nav channel slow inactivation and reveal a

mechanism that supports cortical resilience to pathological perturbations.

Introduction

Voltage-gated sodium (Nav) channels are critical for the initiation and propagation of electrical signals in excitable cells, contributing to cellular excitability in various tissues(Hodgkin & Huxley, 1952; Ulbricht, 1977). In mammals, including humans, Nav channels consist of nine □ subunit isoforms (Nav1.1-Nav1.9), which are differentially expressed and distributed across different tissues to regulate specific physiological functions(Catterall, Goldin, & Waxman, 2005). Mutations in Nav channels that lead to either loss- or gain-of-function of these channels are associated with a wide spectrum of diseases, including neurological disorders(Escayg & Goldin, 2010; Hedrich, Lauxmann, & Lerche, 2019; Meisler, Hill, & Yu, 2021), pain syndromes(Dib-Hajj, Geha, & Waxman, 2017; Waxman, 2013), muscle illnesses(Cannon, 2018; Mantegazza, Cestele, & Catterall, 2021) and cardiac diseases(Remme, 2013). Consequently, the Nav channels are considered promising therapeutic targets for treating these conditions(Noreng, Li, & Payandeh, 2021; Wisedchaisri & Gamal El-Din, 2022).

Voltage-dependent conformational changes enable Nav channels to transition between resting, open and inactivated states(Catterall, Wisedchaisri, & Zheng, 2020). Eukaryotic Nav channels undergo two major forms of inactivation (fast and slow inactivation), which are distinguished by their kinetics of onset and recovery(Goldin, 2003). Fast inactivation is triggered within milliseconds by brief depolarization and is rapidly reversed upon hyperpolarization, typically within tens of milliseconds (Armstrong & Bezanilla, 1977; Bezanilla & Armstrong, 1977). In contrast, slow inactivation develops during prolonged depolarizations and the slow inactivated channels require substantially longer periods to recover, ranging from hundreds of milliseconds to minutes(Rudy, 1978). Previous studies have demonstrated that slow inactivation regulates Nav channel availability during sustained or repetitive depolarization, thus modulating the cellular excitability(Goldin, 2003; Silva, 2014; Vilin & Ruben, 2001). Impairment of this regulatory process due to the mutations in Nav channels has been associated with disorders such as periodic paralysis(Hayward, Sandoval, & Cannon, 1999), cardiac arrhythmias(Richmond, Featherstone, Hartmann, & Ruben, 1998; Vilin, Makita, George, & Ruben, 1999) and epilepsy(Ghovanloo et al., 2023).

Beyond the intrinsic hierarchical gating mechanisms, auxiliary regulators further modulate Nav channel inactivation dynamics(Goldin, 2003). For example, β subunits of sodium channels (SCN1B) regulate inactivation of Nav channels in the heterologous expression system, although their effects vary across different Nav isoforms and cell types(He & Soderlund, 2014; Vilin et al., 1999; Webb, Wu, & Cannon, 2009). Fibroblast growth factor homologous factors (FHFs) interact with the carboxy terminus of Nav channels(Gade, Marx, & Pitt, 2020; Goetz et al., 2009), promoting intermediated or long-term inactivation, with recovery times spanning hundreds of milliseconds(Dover, Solinas, D'Angelo, & Goldfarb, 2010; Venkatesan, Liu, & Goldfarb, 2014). Although these auxiliary proteins have been identified as regulators of fast or intermediate inactivation, native modulators that specifically targeting slow inactivation of Nav channels remain largely unknown.

Recent studies on proline-rich transmembrane protein 2 (PRRT2) provide new insights into this issue. The *PRRT2*, a member of the Dispanins B subfamily (DspB)(Sallman Almen, Bringeland, Fredriksson, & Schioth, 2012), has been identified as a causative gene for paroxysmal kinesigenic dyskinesia disease(W. J. Chen et al., 2011; Lee et al., 2012; J. L. Wang et al., 2011). *In vitro* studies have shown that PRRT2 regulates Nav channel surface expression and delays recovery of these channels from inactivated states induced by brief depolarization(Fruscione et al., 2018; Lu et al., 2021; Valente et al., 2023). However, these studies did not clearly distinguish between the effects of PRRT2 on fast versus slow inactivation, nor did they provide direct *in vivo* evidence for its role in regulating Nav channel inactivation. Our original observations that PRRT2 expression increased the accumulation of inactivated Nav channels during repetitive stimulation(Lu et al., 2021) suggest that PRRT2 may be a previously unrecognized auxiliary regulator of Nav channel slow inactivation.

In this study, we combined whole-cell voltage-clamp recordings, co-immunoprecipitation, and *in vivo* approaches to investigate the role of PRRT2 in regulating Nav channel slow inactivation, and to examine how deficits in PRRT2-mediated modulation of this process affects neuronal function in awake mice.

Results

PRRT2 regulates the slow inactivation of Nav1.2 channels

Fast and slow inactivation of Nav channels proceed through distinct gating pathways(Goldin, 2003). Although previous studies have implicated PRRT2 in the regulation of Nav channel inactivation(Fruscione et al., 2018; Lu et al., 2021), it remains unclear whether PRRT2 primarily influences fast inactivation, slow inactivation or both. To address this, we express mouse PRRT2 in HEK293T cells stably expressing Nav1.2 (Figure 1A) and applied classic electrophysiological paradigms to distinguish between the two inactivation processes.

Fast inactivation of Nav channels is rapidly triggered by brief depolarization and manifests as a current decay following a transient pore opening (Figure 1B), consistent with previous reports(Misra, Kahlig, & George, 2008; Thompson et al., 2023). To evaluate the kinetics of fast inactivation, we measured the time constant of current decay and found that PRRT2 expression did not significantly alter the rate at which Nav channels entered the fast-inactivated state (Figure 1C). Moreover, the majority of Nav1.2 channels recovered from fast inactivation within ~10 ms at a hyperpolarized potential of -120 mV, and PRRT2 expression had a minimal effect on this recovery (Figure 1D).

In contrast to fast inactivation, Nav channel slow inactivation develops and recovers over much longer timescales (Figure 1E), typically ranging from hundreds of milliseconds to seconds, or even to minutes(Silva, 2014). Because slow-inactivated channels do not recover during brief hyperpolarization, they can be functionally distinguished from fast-inactivated channels using a classic two-pulse protocol. In this approach, a brief hyperpolarization step (e.g., -120 mV, 10 ms) is inserted between a conditioning pulse and a test pulse to recover fast-inactivated channels. Channels that have entered the slow-inactivated state remain unavailable during the test pulse, resulting in a reduction in peak sodium current (Figure 1E)(Featherstone, Richmond, & Ruben, 1996).

To assess the development of slow inactivation, we applied depolarization pulses of variable duration, followed by a fixed 10-ms hyperpolarization before the test pulse (Figure 1F). We found that a 5-second depolarization at 0 mV was sufficient to drive most Nav1.2 channels into the slow-inactivated state (Figure 1F), consistent with previous studies(Ganguly, Thompson, & George, 2021). PRRT2 significantly promoted the entry of Nav1.2 channels into the slow-inactivated state during sustained depolarization (Figure 1F).

To examine the role of PRRT2 in channel recovery from slow inactivation, we used a protocol in which a fixed 5-second depolarization at 0 mV was followed by varying durations of hyperpolarization at -120 mV to allow channel repriming (Figure 1G). PRRT2 expression markedly slowed the recovery of Nav channels from the slow-inactivated state (Figure 1G).

To further investigate whether the regulation of PRRT2 in slow inactivation is voltage dependent, we performed a steady-state slow inactivation protocol. In this assay, 10-s depolarizing steps from -110 to -10 mV were applied to drive Nav channels into steady state, followed by a fixed hyperpolarization and a test pulse to assess channel availability (Figure 1-figure supplement 1A). We found that PRRT2 promotes the transition of Nav channels into the slow-inactivated state across a broad range of membrane potentials. PRRT2 expression induced a pronounced hyperpolarizing shift in the inactivation curve, with a $V_{0.5}$ of -76.27 mV compared to -48.05 mV in controls (Figure 1-figure supplement 1B). Together, these findings indicate that PRRT2 is a potent regulator of Nav1.2 channel slow inactivation *in vitro*.

Functional auxiliary factors in the regulation of Nav channel slow inactivation

Several auxiliary factors of Nav channels have been identified, including the SCN1B and FHF2A (also known as FGF13a), both of which are implicated in modulating Nav channel inactivation(Dover et al., 2010; Isom et al., 1992). In this study, we compared the effects of mouse SCN1B and FGF13a with those of PRRT2 on the development and recovery of Nav channel slow inactivation (Figure 2A).

We found that SCN1B had negligible effects on both the entry into and recovery from the slow-inactivated state of Nav1.2 compared to controls (Figures 2B and C). In contrast, FGF13a markedly accelerated the onset of inactivation (Figure 2B), consistent with previous reports(Dover et al., 2010; Venkatesan et al., 2014). Notably, FGF13a had minimal effect on the recovery of Nav channels from the slow-inactivated state induced by a 5-second depolarization (Figure 2C). These distinct effects of FGF13a on inactivation suggest that FGF13a does not modulate classical slow inactivation, but rather promotes a form of rapid-onset and long-term inactivation(Dover et al., 2010; Venkatesan et al., 2014). By comparison, PRRT2 uniquely regulated slow inactivation by both facilitating entry into and delaying recovery from the slow-inactivated state of Nav channels (Figures 2B and C).

The rodent *Prrt2* gene encodes a 346-amino-acid protein containing a proline-rich domain in the N-terminus, a re-entrant loop, and a transmembrane domain in the C-terminus (Figure 2D). To identify the functional domain(s) responsible for regulating slow inactivation, we generated a series of protein-truncating variants (Figure 2D).

We first examined PRRT2(222–346), which lacks the N-terminal proline-rich domain (Figure 2D). This variant retained activity similar to the full-length PRRT2, enhancing slow inactivation development and delaying recovery (Figures 2E and F). A shorter construct, PRRT2(256–346), which retains the intact C-terminus, also preserved regulatory function in modulating slow inactivation compared to the EGFP control (Figures 2E and F). To further test whether the C-terminal region is necessary for the effect of PRRT2 on Nav channel slow inactivation, we examined PRRT2(1–266), a truncated variant lacking the membrane-associated C-terminal domains (Figure 2D). Unlike variants containing the C-terminal region, PRRT2(1–266) showed no detectable effect on either the development or recovery of Nav channel slow inactivation compared to the control (Figures 2E and F).

Together, these results indicate that the C-terminal region of PRRT2, including the re-entrant loop and transmembrane domain, is both necessary and sufficient to mediate its regulatory effect on slow inactivation of Nav1.2 channels *in vitro*.

Evolutionarily conserved effects of PRRT2 on Nav channel slow inactivation

The *PRRT2* and *PRRT2*-like genes emerged in vertebrates and have been conserved throughout evolution(Sallman Almen et al., 2012). The alignment of amino acid sequences from zebrafish, mouse, and human PRRT2 revealed 77.46% identity between human and mouse PRRT2, and 43.60% identity between zebrafish and mouse PRRT2 (Figures 3A and 3B). Notably, the majority of conserved residues are located within the C-terminal region of the PRRT2 proteins (Figure 3A). Given the essential role of the C-terminus of mouse PRRT2 in regulating Nav channel slow inactivation, we examined whether PRRT2 proteins from different species exhibit similar effects.

By comparing the effects of zebrafish, mouse, and human PRRT2 on Nav channel slow inactivation, we found that all three PRRT2 orthologs similarly promoted the entry of Nav1.2 channels into the slow-inactivated state (Figure 3C). Surprisingly, in recovery assays, zebrafish PRRT2 was more effective at delaying the recovery process compared to its mammalian

counterparts (Figure 3D). To identify the determinant domain of zebrafish PRRT2 for this enhanced effect, we generated a chimeric PRRT2 construct by fusing the C-terminal region of zebrafish PRRT2 to the N-terminal region of human PRRT2 (Figure 3E). The chimeric PRRT2 exhibited comparable effects on the rate of slow inactivation development to those observed with both human and zebrafish PRRT2 (Figure 3F). Notably, the chimeric variant displayed enhanced modulation of recovery, resembling zebrafish PRRT2 and significantly differing from human PRRT2 (Figure 3G). These findings indicate that C-terminal region of zebrafish PRRT2 confers its greater ability to modulate recovery of Nav1.2 from slow-inactivated state.

We next extended our analysis to other DspB family members, including *Trafficking regulator of GLUT4-1* (*trarg1*) and *Transmembrane protein 233* (*tmem233*), both of which encode proteins with C-terminal regions similar to that of PRRT2 (Figure 3-figure supplement 2A and B). Given the critical role of the PRRT2 C-terminus in modulating slow inactivation, we hypothesized that TRARG1 and TMEM233 might exert similar regulatory effects. Under heterologous expression conditions, both TRARG1 and TMEM233 facilitated the entry of Nav1.2 channels into the slow-inactivated state and delayed their recovery (Figure 3-figure supplement 2C and D). These effects were comparable to those observed with mouse PRRT2, although TMEM233 exhibited slightly weaker modulation than PRRT2 and TRARG1 (Figure 3-figure supplement 2C and D).

Together, these results suggest that the role of PRRT2 in regulating Nav channel slow inactivation is evolutionarily conserved.

Uniform influence of PRRT2 on slow inactivation across human Nav isoforms

In humans, the nine Nav channel isoforms (Nav1.1-1.9) share high sequence homology and similar structural features(Goldin, 2001). To investigate whether PRRT2 modulates slow inactivation across different Nav channel isoforms, we selected Nav1.1, Nav1.4, and Nav1.5, which are expressed in distinct tissues, and assessed the effects of human PRRT2 on their slow inactivation properties (Figures 4A-H).

Both Nav1.1 and Nav1.4 exhibited similar kinetics in the development and recovery of slow inactivation (Figures 4B, C, F and G). In contrast, Nav1.5 showed greater resistance to entering the slow-inactivated state (Figures 4D and H), consistent with previous findings(Richmond et al., 1998). Despite these isoform-specific differences, the heterologous expression of

PRRT2 consistently promoted entry of Nav channels into the slow-inactivated state (Fig. 4A-D) and delayed recovery from it (Figures 4E-H) across all three Nav isoforms tested. These results suggest that PRRT2 modulates slow inactivation through a common mechanism shared by multiple isoforms of Nav channels.

To assess whether the regulatory effect of PRRT2 on slow inactivation is specific to Nav channels, we further examined its influence on the A-type voltage-dependent potassium channel, Kv1.4 (Figure 4-figure supplement 3A). Kv1.4 exhibits two types of inactivation: N-type and C-type, which are functionally analogous to the fast and slow inactivation observed in mammalian Nav channels(Hoshi, Zagotta, & Aldrich, 1990). Unlike Nav channels, where fast and slow inactivation can be temporally separated, C-type inactivation in Kv1.4 cannot be clearly isolated from N-type inactivation due to the relatively slow recovery kinetics of the latter(Bett, Dinga-Madou, Zhou, Bondarenko, & Rasmusson, 2011). Given this limitation, we employed a modified assay that did not distinguish between N- and C-type inactivation. Using this protocol, we found that PRRT2 has negligible effects on both the entry into and recovery from the inactivated state of Kv1.4 (Figure 4-figure supplement 3B and C). Since recovery from inactivation in Kv1.4 is primarily governed by C-type inactivation(Bett et al., 2011), this lack of effect suggests that PRRT2 does not modulate slow inactivation in Kv1.4.

Together, these findings indicate that PRRT2 selectively regulates slow inactivation in Nav channels but does not influence inactivation in Kv1.4, supporting the channel-type specificity of PRRT2 function.

Intermolecular interaction between PRRT2 and Nav channels *in vitro*

PRRT2 may regulate slow inactivation by interacting with Nav channels. To examine the potential physical association between human PRRT2 and Nav1.2, we co-expressed PRRT2-HA and Flag-Nav1.2 in HEK293T cells and performed co-immunoprecipitation (co-IP) assays (Figures 5A and B). As controls, cells were transfected with one of the two interacting proteins (either PRRT2-HA or Flag-Nav1.2) together with the empty vectors carrying the corresponding tag of the other protein (Figures 5A and B). Immunoprecipitation using an anti-Flag antibody to capture Flag-Nav1.2 successfully co-precipitated PRRT2 in the co-transfection group, but not in the control groups where either protein was expressed (Figure 5A). Conversely, immunoprecipitation with anti-HA antibody showed that Nav1.2 was specifically co-

precipitated with PRRT2-HA in the co-transfection group but not in controls (Figure 5B). These results confirm that PRRT2 and Nav1.2 formed a protein complex *in vitro*.

To identify the Nav1.2-binding domain within human PRRT2, we generated truncated constructs encoding either the N-terminus (residues 1–268 amino acid) or C-terminus (residues 250–340 amino acid) of PRRT2. Using the same co-IP approach, we found that PRRT2(1–268), which contains the intracellular proline-rich domain, failed to interact with Nav1.2 (Figures 5C-E). In contrast, the PRRT2(250–340), which includes the re-entry loop and transmembrane domain, was able to bind Nav1.2 (Figures 5F-H). These results demonstrate that C-terminal region of PRRT2 is both necessary and sufficient for interacting with Nav1.2 channels.

Given that PRRT2 modulates slow inactivation across multiple Nav isoforms, we hypothesized that it could interact with other Nav isoforms, such as Nav1.1. To test this, we co-expressed PRRT2-HA and Flag-Nav1.1 in HEK293T cells and performed co-IP assays. Under these conditions, PRRT2 was found to interact with Nav1.1 (Figures 5I and J), similar to the interaction observed with Nav1.2 (Figures 5A and B).

These findings contrast with previous reports, which reported that PRRT2 preferentially interacted with Nav1.2 over Nav1.1 *in vitro*(Franchi et al., 2023; Fruscione et al., 2018; Valente et al., 2023). This discrepancy may stem from differences in the experimental conditions used to assess protein-protein interactions. For example, in our study, Nav1.1 and PRRT2 were co-expressed in HEK293T cells, and cells were solubilized using the detergent n-Dodecyl β-D-maltoside (DDM). Variations in experimental conditions could influence the stability of PRRT2-Nav channel complex and the efficiency of Co-IP assay.

Collectively, our findings suggest that PRRT2 interacts directly with Nav channels through its membrane-associated C-terminal domains, forming molecular complexes *in vitro*.

PRRT2 forms a molecular complex with Nav1.2 in the mouse brain

To extend our findings from the heterologous expression system to an *in vivo* context, we first investigated whether PRRT2 forms a protein complex with Nav channels in brain tissue. Due to the limited efficacy of available antibodies for immunoprecipitating native PRRT2 or Nav1.2 from brain lysates, we employed a tag-based capture strategy, which relies on the appropriate insertion of a commonly used epitope tag into the target protein.

We generated *Prrt2-V5* knock-in mice via CRISPR/Cas9 technology(Yang, Wang, & Jaenisch, 2014), in which a V5 epitope tag was inserted at the C-terminus of PRRT2 (Figures 6A and B). Notably, compared to wild-type mice, PRRT2 protein levels in lysates were markedly reduced in *Prrt2-V5* knock-in mice, likely due to the insertion of V5 tag, whereas Nav1.2 expression remained unchanged (Figures 6C-E). Despite the reduced PRRT2 expression, co-immunoprecipitation assays were effective. Using anti-V5 nanobody-conjugated magnetic beads, PRRT2 was effectively immunoprecipitated from membrane lysates of brain tissue (Figure 6C). A notable amount of Nav1.2 were co-immunoprecipitated in the *Prrt2-V5* knock-in group, whereas only trace levels were detected in wild-type controls (Figures 6C and F). In contrast, ATP1B2, another membrane protein, was not co-immunoprecipitated in the *Prrt2-V5* group (Figures 6C and F), indicating that the interaction between PRRT2 and Nav1.2 is specific. Together, these results provide *in vivo* evidence that PRRT2 forms a molecular complex with Nav1.2 channels in the mouse brain.

PRRT2 deficiency impairs the regulation of Nav channel slow inactivation in cortical neuronal axons

Given the dense distribution of both PRRT2 and Nav channels in the cerebral and cerebellar cortices(Yamano, Miyazaki, & Nukina, 2022), we next investigated whether PRRT2 regulates Nav channel slow inactivation in cortical neurons. Cortical slices were prepared from wild-type and *Prrt2*-mutant mice, the latter lacking PRRT2 expression(Tan et al., 2018). Unlike the relatively simple morphology of HEK293T cells, pyramidal neurons have complex arborizations, which present space-clamp limitations during whole-cell voltage-clamp recordings(Bar-Yehuda & Korngreen, 2008). To mitigate these issues, we followed established protocols to isolate axonal blebs from cortical pyramidal neurons(Hu & Shu, 2012). These spherical, membrane-bound blebs form at the cutting surface of cortical slices and are readily visualized (Figure 7A). Sodium currents recorded from axon blebs were voltage-dependent and sensitive to tetrodotoxin (TTX), confirming that they were primarily mediated by Nav channels(Hu & Shu, 2012).

PRRT2 deficiency did not affect Nav1.2 protein expression in forebrain tissues (Figure 7-figure supplement 4A and B), nor did it alter the sodium current density in cortical axonal blebs (Figure 7B). Because long-term voltage-clamp recordings from isolated axonal bleb are

technically challenging, we employed a simplified protocol to assess Nav channel slow inactivation, using a holding potential of -70 mV to approximate the resting membrane potential of cortical neurons. In this protocol, a single 5-s depolarization to 0 mV was applied, and the fraction of available Nav channels was determined after a 10-ms hyperpolarization (Figure 7C).

Approximately 20% of Nav channels in wild-type blebs remained available, compared to ~40% *Prrt2*-mutant blebs (Figures 7C and D), indicating that during sustained depolarization, fewer Nav channels in the *Prrt2*-mutant group entered the slow-inactivated state. Notably, because the proportion of channels entering slow inactivation differed substantially between wild-type and *Prrt2*-mutant groups, direct comparison of recovery kinetics was not feasible and was therefore not performed. Nevertheless, these findings provide direct evidence that endogenous PRRT2 is required for effective regulation of Nav channel slow inactivation in cortical neurons.

PRRT2 deficiency compromises cortical resilience in awake mice

Slow inactivation of Nav channels is essential for limiting neuronal excitability during episodes of aberrant hyperactivity in the neuronal networks(Zang, Marder, & Marom, 2023). Given the ability of PRRT2 to regulate this process, we hypothesized that PRRT2 might contribute to cortical resilience in awake mice, a property reflecting the resistance of the cerebral cortex to pathological perturbations.

To assess this, we employed a stimulation-response paradigm in which stimulation electrodes were implanted into the left hemisphere of the cerebral cortex, targeting both the sensory and visual cortices, while EEG recording electrodes were placed in the contralateral hemisphere that receives projections from the stimulation region (Figure 7E). We applied pulsed electrostimulations (1-ms width at 60 Hz for 2 s) to the cortex of mice once daily with stepwise increases in intensity, and the minimal current required to evoke after-discharges (ADs) in the contralateral cortex was determined in each animal (Figure 7F). The current threshold required to induce after-discharges serves as a functional indicator of cortical resilience to aberrant excitatory inputs(Blume, Jones, & Pathak, 2004).

Prrt2-mutant mice exhibited significantly lower stimulation thresholds for evoking after-discharges compared to wild-type controls (Figures 7G and H). Specifically, stimulation at an

average intensity of 85 μA reliably induced after-discharges in *Prrt2*-mutant mice, whereas a significantly higher intensity (190 μA) was required to elicit similar responses in wild-type mice (Figures 7H and I), suggesting that PRRT2 is essential for maintaining cortical resilience in response to excitatory perturbations.

Discussion

In this study, we identified PRRT2 as a crucial auxiliary factor of Nav channel slow inactivation. We demonstrate that PRRT2 exerts a dual action by both facilitating the transition of Nav channels into a slow-inactivated state and delaying their recovery. Importantly, this regulatory action is evolutionarily conserved, and requires the integrity of the PRRT2's C-terminal region. Using both *Prrt2-V5* knock-in and *Prrt2*-mutant mouse models, we provide compelling evidence that PRRT2 forms a molecular complex with Nav channels *in vivo* and plays an essential role in modulating their slow inactivation, thereby contributing to the maintenance of neuronal resilience to perturbations.

In eukaryotic Nav channels, ion permeability is regulated through at least four distinct and coordinated gating mechanisms: voltage-gated activation and deactivation, fast inactivation, and slow inactivation(Catterall, 2023). Slow inactivation, an evolutionarily conserved intrinsic property of Nav channels, is mediated by conformational rearrangements and has distinct molecular determinants from those governing fast inactivation(Payandeh, 2018; Silva, 2014; Vilin & Ruben, 2001).

Previous studies have suggested that slow inactivation involves conformational changes at multiple structural regions of the Nav channels. The external pore mouth(Balser et al., 1996; Xiong et al., 2006), the selectivity filter(Chatterjee et al., 2018; Todt, Dudley, Kyle, French, & Fozzard, 1999), the S6 segments(Chancey, Shockett, & O'Reilly, 2007; Y. Chen, Yu, Surmeier, Scheuer, & Catterall, 2006; S. Y. Wang & Wang, 1997), and the regions within S4, S4-S5 linker and S5 segments(Bendahhou, Cummins, Kula, Fu, & Ptacek, 2002; Cummins & Sigworth, 1996; Hayward et al., 1999; Mitrovic, George, & Horn, 2000; D. W. Wang, Makita, Kitabatake, Balser, & George, 2000), have been implicated in modulating slow inactivation of Nav channels. The present study did not directly verify whether these structural regions mediated the effect of PRRT2 on Nav channel slow inactivation. However, insights from molecular modeling of protein complex provide valuable clues. By using the recently developed

AlphaFold3(Abramson et al., 2024), we modeled a putative interaction between PRRT2 and the Nav channel. The predicted complex suggests that the C-terminal region of PRRT2 interacts with the S3 segment of domain IV (DIV-S3) of Nav isoforms. This raises the possibility that residues within DIV-S3 may serve as critical determinants for the regulatory effects of PRRT2 on Nav channel slow inactivation.

The role of PRRT2 in the regulation of Nav channel slow inactivation appears to be unique compared to known regulators such as SCN1B and FHFs. The modulatory effects of the SCN1B on Nav channel inactivation were initially observed in *Xenopus* oocytes(Wallner, Weigl, Meera, & Lotan, 1993), where it was found to influence sodium currents. Subsequent studies proposed that the SCN1B impedes slow inactivation, a hypothesis later confirmed in mammalian cells co-expressing Nav1.4 and SCN1B(Webb et al., 2009). However, its regulatory effects on slow inactivation were varied across Nav isoforms(He & Soderlund, 2014; Makita, Bennett, & George, 1996; Vilin et al., 1999; Xu et al., 2007). In this study, we observed little effect of SCN1B on the onset and recovery of slow inactivation in Nav1.2, consistent with previous findings(Xu et al., 2007). In contrast to SCN1B, PRRT2 exerts a more consistent effect across Nav isoforms, enhancing slow inactivation regardless of the specific Nav subtype.

FHF proteins (FHF1-4, also known as FGF11-14) constitute a subfamily of FGFs that lack a secretion signal and function distinctly from traditional FGFs(Olsen et al., 2003). Previous studies demonstrated that FHFs mediate a rapid-onset, long-term inactivation, which differs mechanically from traditional slow inactivation(Dover et al., 2010). Unlike the FHF2A-mediated long-term inactivation, which can be triggered by a brief 2-ms depolarization, PRRT2 requires a longer depolarization to affect the onset of slow inactivation of Nav channels. Additionally, PRRT2 significantly delays the Nav channel recovery from slow inactivation induced by 5-second depolarization, whereas FHF2A has little effect on this process. These findings suggest that PRRT2 and FHF2A modulate Nav channel inactivation through different mechanisms.

In mammals, Nav channel isoforms (Nav1.1–1.9) are distributed across the nervous system, skeletal muscle, heart and secretory glands(Cusdin, Clare, & Jackson, 2008). Although we have shown that PRRT2 exerts a consistent effect on slow inactivation across various Nav

channel isoforms *in vitro*, the regulation of Nav channel slow inactivation is likely to be more complex under physiological conditions. PRRT2 is predominantly expressed in the nervous system(W. J. Chen et al., 2011), with enrichment in excitatory neurons(Tan et al., 2018), making it unlikely to directly modulate Nav1.4 and Nav1.5 channels, which are primarily expressed in skeletal muscle and cardiac tissue, respectively(Cusdin et al., 2008). A similar rationale applies to Nav1.1, which is largely confined to inhibitory interneurons(Yu et al., 2006), where PRRT2 expression is minimal or absent.

The partial mismatch between PRRT2 and Nav channel expression *in vivo* raises an important question that how Nav channel slow inactivation is regulated in cells that do not express PRRT2. One possibility is the expression of alternative regulators, such as TRARG1 or TMEM232, both of which belong to the DspB family and are expressed in tissues distinct from PRRT2(Ehrlich, Lacey, & Ehrlich, 2020; Oort, Warden, Baumann, Knotts, & Adams, 2007; Santana-Varela et al., 2021; Shibata et al., 2007). These proteins may serve analogous functions in modulating Nav channel slow inactivation. Another possibility is that certain PRRT2-negative cells have a reduced requirement for Nav channel slow inactivation modulation due to their intrinsic rhythmic firing properties. For instance, in the cerebellar cortex, the PRRT2 is absent in Purkinje cells, which exhibit repetitive firing(Lu et al., 2021). In such rhythmic firing cells, strong regulation of Nav channel slow inactivation may be undesirable, as excessive accumulation of inactivated Nav channels could disturb the regular firing patterns of these cells.

Given the critical role of PRRT2 in regulating Nav channel slow inactivation, its deficiency is expected to alter neuronal responses to intense and prolonged activity, thereby contributing to dysfunction in the central nervous system. Evidence from both animal models and clinical studies supports this hypothesis. In the present study, we found that PRRT2 deficiency impairs slow inactivation of Nav channels in cortical neurons, leading to reduced resistance to pathological perturbations, as evidenced by an increased susceptibility to after-discharge induction in awake mice. Previous studies have also reported that loss-of-function mutations or knockout of PRRT2 increase intrinsic excitability in cerebellar granule cells and promote spreading depolarization in the cerebellar cortex(Binda, Valente, Marte, Baldelli, & Benfenati, 2021; Lu et al., 2021). In humans, *PRRT2* mutations are associated with infantile

convulsions(Lee et al., 2012), paroxysmal dyskinesia(W. J. Chen et al., 2011; J. L. Wang et al., 2011), and hemiplegic migraine(Riant et al., 2022), all of which are linked to dysfunction in neuronal network excitability. Based on these lines of evidence, we conclude that PRRT2 deficiency in excitatory neurons impairs Nav channel slow inactivation, thereby compromising neuronal resilience to aberrant excitability and ultimately contributing to these episodic neurological disorders.

Together, the identification of PRRT2 as an auxiliary factor regulating Nav channel slow inactivation has significant implications for understanding the fine-tuning mechanisms of Nav channel function. Additionally, these findings may inform the development of novel therapeutic strategies for treating neurological disorders associated with excitability dysregulation.

Limitations of the study

While our study successfully identifies the functional domain of PRRT2, the specific interaction site on the Nav channel that binds PRRT2 and mediates the regulation of slow inactivation remains unknown. Further investigations are required to map the PRRT2 binding region on Nav channels and to determine how mutations at these sites influence PRRT2-dependent modulation of slow inactivation. Cryo-electron microscopy (cryo-EM) is a promising approach for resolving the structural details of the Nav-PRRT2 complex, particularly given recent advancements in determining high-resolution structures of various Nav channel isoforms and their complexes with auxiliary factors(Jiang et al., 2020; Pan et al., 2019; Pan et al., 2021). A detailed structural characterization of the Nav-PRRT2 interaction would provide critical insights into the molecular mechanisms governing Nav channel slow inactivation.

Materials and Methods

Molecular cloning

Mammalian expression constructs were generated using the pCAGIG backbone (Addgene, 11159), which contains an internal ribosome entry site (IRES) followed by EGFP(Matsuda & Cepko, 2004). Coding sequences for full-length or truncated protein-of-interests (POIs) were inserted in the pCAGIG vector using a seamless cloning method (Beyotime, D7010). The POIs including human PRRT2 (hPRRT2), hPRRT2(1–268), hPRRT2(250–340), mouse PRRT2 (mPRRT2), mPRRT2(222–346), mPRRT2(256–346), mPRRT2(1–266), zebrafish PRRT2 (zfPRRT2), mouse SCN1B, mouse FHF2A, mouse TRARG1 and mouse TMEM233.

A PRRT2 chimeric construct was generated by fusing the N-terminal fragment of human PRRT2 (hPRRT2(1–222)) with the C-terminal region of zebrafish PRRT2 (zPRRT2(110–226)), and cloning the resulting sequence into pCAGIG vector. Plasmids encoding human PRRT2(W. J. Chen et al., 2011) were kindly provided by Dr. Zhi-Ying Wu's Laboratory (Zhejiang University). Plasmids of pCAG-Flag-Nav1.2(Pan et al., 2019) and pCAG-Flag-Nav1.1(Pan et al., 2021) were provided by Huai-Zong Shen's Laboratory (Westlake University). All constructs generated in this study were verified by Sanger sequencing (BioSune, Boshang Biology Technology, Shanghai).

Cell culture and heterologous expression

HEK293T cell lines stably expressing human Nav1.2 or Kv1.4 respectively and CHO cell lines stably expressing human Nav1.1, Nav1.4 or Nav1.5 were obtained from the laboratory of ICE Bioscience Inc. Wild-type HEK293T cells (SCSP-502) used for transient transfection were obtained from Cell Bank/Stem Cell Bank of Chinese Academy of Sciences. All cells were cultured in Dulbecco's modified Eagle medium (DMEM; Gibco, 11995065) supplemented with 10% fetal bovine serum (FBS; Gibco,10099141) and penicillin (50 U/mL)-streptomycin (50 μg/mL) (Gibco,15140163), and maintained at 37 °C in a humidified incubator with 5% CO_2. The HEK293T cell line used in this study is of female origin and tested negative for mycoplasma contamination.

For heterologous protein expression in whole-cell voltage-clamp recording, 2 μg of plasmid DNA was transfected into HEK293T or CHO cells using Lipofectamine 2000 (ThermoFisher, 11668-019) according to the manufacturer's instructions. For co-immunoprecipitation assays, 2–3 μg of total plasmid DNA (encoding two proteins of interest) was used for co-transfection. Four hours after the transfection, the medium was replaced with fresh growth medium, and cells were maintained for an additional 20 hours before subsequent experiments.

Animals

Prrt2-mutant mice, carrying a premature stop codon in exon 2 of the *Prrt2* gene(Tan et al., 2018), were used in electrophysiological recording experiments.

Prrt2-V5 knock-in mice, used for co-immunoprecipitation (Co-IP) experiments, were generated in this study via CRISPR/Cas9 technology(Yang et al., 2014). Briefly, single-guide RNA (sgRNA: 5'-TCTCCCACAGTGTATAAGTG-3') targeting the location nearby the stop codon of

Prrt2 gene allele, together with a single-stranded DNA donor template encoding a V5 tag flanked by 53-bp homology arms (ssDNA: 5'-CTTCCCTGTC TGTCTTTCCC TCTCCTCTCC CACAGTGTAT AAGGGCAAGC CCATCCCCAA CCCCCTGCTG GGCCTGGACA GCACCTGAGG GGCTCTGCCC TGCATTCCAA GACTTTTCTT CCTGTTGG-3') and Cas9 mRNA, were microinjected into zygotes from fertilized C57BL/6J mice. The injected zygotes were implanted into pseudopregnant female mice. Offspring were screened for correct insertion of the V5 tag immediately upstream of the *Prrt2* stop codon by PCR, and the insertion was subsequently verified by Sanger sequencing. Positive founder (F0) mice were crossed with C57BL/6J mice to establish the *Prrt2-V5* knock-in line.

Both *Prrt2*-mutant and *Prrt2-V5* lines were backcrossed onto the C57BL/6J background for more than 10 generations. C57BL/6J mice used for breeding were obtained from the Shanghai Laboratory Animal Center (SLAC), Chinese Academy of Science.

Mice were housed in a 12-h light-dark cycle (light on at 7:00 a.m.) with ad libitum access to food and water. All procedures involving animals were approved by the Animal Care and Use Committee of the Center for Excellence in Brain Science and Intelligence Technology, Chinese Academy of Sciences (Approval number, NA-009-2022). Both male and female mice were used in experiments.

Whole-cell voltage clamp recording for sodium currents in cell lines

Sodium currents were recorded from HEK293T or CHO cell lines stably expressing individual human Nav channel isoforms (ICE Bioscience Inc.). Cells were transfected with plasmids as described in the main text. Twenty-four hours after transfection, cells were trypsinized and replated at lower density onto poly-D-lysine-coated coverslips. EGFP-positive cells were selected for recording 24 hours later.

Whole-cell voltage-clamp recordings were conducted at room temperature (23-24 °C). The bath solution contained (in mM): 50 NaCl, 90 choline chloride, 3.5 KCl, 1 $MgCl_2$, 2 $CaCl_2$, 10 D-Glucose, 1.25 NaH_2PO_4, and 10 HEPES (pH adjusted to 7.4 with NaOH). The internal pipette solution contained (in mM): 50 CsCl, 60 CsF, 10 NaCl, 20 EGTA, 10 HEPES (pH adjusted to 7.2 with CsOH). The osmolarity of the external and internal solutions was adjusted to 300 and 290 mOsmol/kg, respectively.

Pipette electrodes were pulled from borosilicate glass capillary (Sutter Instruments, BF150-

86-10) using a horizontal puller (P-97, Sutter Instruments). The pipette resistance was approximately 2 MΩ when filled with internal pipette solution. After whole-cell configuration was achieved, cells were allowed to equilibrate for 5 minutes prior to recording. Series resistance was compensated by 80% to minimize voltage errors. Currents were recorded with an amplifier (HEKA, EPC-10), sampled at 10 kHz, and acquired using Patchmaster (HEKA, v2x92).

Fast inactivation assay for Nav channels

To assess the fast inactivation kinetics of Nav channels, sodium currents were evoked by 20-ms depolarizing pulse to 0 mV from a holding potential of -120 mV. The time constant (tau) of current decay was obtained by mono-exponential fitting of the current trace.

Recovery from fast inactivation was measured using a two-pulse protocol, in which a 10-ms depolarizing pulse to 0 mV (P1) was followed by a variable-duration recovery period at -120 mV and a second 10-ms test pulse at 0 mV (P2). Recovery was quantified as the normalized peak current of P2 relative to P1.

Slow inactivation assay for Nav channels

To evaluate the development of slow inactivation of Nav channels, a series of conditioning prepulses of increasing duration at 0 mV was applied, followed by a brief 10-ms recovery at -120 mV and a 10-ms test pulse at 0 mV. Inter-sweep intervals were set at 15 s. Available fractions of Nav channels were assessed by normalizing the peak currents in the test pulse to that of the conditioning pulse.

For slow inactivation recovery, a 5-s conditioning pulse at 0 mV was followed by variable recovery durations at -120 mV, then a 10-ms test pulse at 0 mV. Inter-sweep interval was 15 s. In experiments assessing the effect of zebrafish PRRT2 on slow inactivation recovery, a modified protocol was used to avoid cumulative inactivation. Within a single sweep, a 5-s depolarization was followed by a series of 10-ms test pulses to 0 mV, each separated by progressively longer recovery periods at -120 mV(Webb et al., 2009).

Steady-state slow inactivation assay for Nav channels

To measure steady-state slow inactivation, 10-s conditioning pulses ranging from -110 to -10 mV (in 10 mV increments) were applied, followed by a 10-ms hyperpolarizing step to -120 mV and subsequently a 5-ms test pulse to 0 mV. The peak test current was normalized to the maximum sodium current recorded across all conditions in the protocol and reported as I/I_{max}.

Whole-cell voltage clamp recording for potassium currents in cell lines

HEK-293 cells stably expressing Kv1.4 channels (ICE Bioscience Inc.) were used to examine the effects of PRRT2 on Kv1.4 channel inactivation. Plasmid transfection and cell preparation were conducted as described in the sodium current recordings section.

For potassium current recording, the external bath solution contained (in mM): 140 NaCl, 3.5 KCl, 1 $MgCl_2$, 2 $CaCl_2$, 10 D-Glucose, 1.25 NaH_2PO_4, 10 HEPES (pH adjusted to 7.4 with NaOH). The internal pipette solution contained (in mM): 20 KCl, 115 K-aspartate, 1 $MgCl_2$, 5 EGTA, 2 Na_2-ATP, 10 HEPES (pH adjusted to 7.2 with KOH).

Inactivation assay for Kv1.4 channels

Unlike Nav channels, the 'fast' (N-type) and 'slow' (C-type) inactivation components of Kv1.4 channels cannot be easily separated by brief hyperpolarization due to the slow recovery kinetics of N-type inactivation. As such, both components were assessed together in this study.

To assess the onset of Kv1.4 inactivation, cells were held at -80 mV and subjected to a series of depolarizing prepulses to +40 mV with increasing durations, followed by a 20-ms test pulse at +40 mV. Inter-sweep interval was 15 s. The fraction of available Kv1.4 channels during the test pulse was calculated by normalizing the peak test current to the peak current during the prepulse step.

To evaluate recovery kinetics, a 5-s depolarizing pulse to +40 mV was applied to induce inactivation, followed by a series of test pulses (40 mV, 20 ms), each separated by progressively increasing recovery periods at -80 mV.

Slice preparation

Mice (postnatal day 14-20) were anesthetized with 4% isoflurane. The brain tissues were rapidly extracted and immersed in ice-cold sucrose-based cutting solution containing (in mM): 2.5 KCl, 1.25 NaH_2PO_4, 26 $NaHCO_3$, 10 $MgSO_4$, 0.5 $CaCl_2$, 10 D-Glucose, 205 sucrose, 1 sodium pyruvate, 1.3 sodium L-ascorbate. Coronal cortical slices (250 μm) were prepared using a vibratome (Leica, VT1200S).

Slices were then transferred immediately to an incubation beaker containing aerated artificial cerebrospinal fluid (ACSF) composed of (in mM): 126 NaCl, 2.5 KCl, 2 $MgSO_4$, 2 $CaCl_2$, 26 $NaHCO_3$, 1.25 NaH_2PO_4 and 25 dextrose (pH 7.4, 315 mOsm). Slices were incubated at 35 °C for 30 min, then maintained in the same solution at room temperature until use. The

oxygenated ACSF was equilibrated with 95% O_2 and 5% CO_2.

Electrophysiological recording in isolated axonal blebs

Slices were transferred to a recording chamber and stabilized with a platinum anchor grid during recording. Resealed axonal ends ("blebs") in the cerebral cortex were visualized using an upright infrared differential interference contrast (IR-DIC) microscope. Individual blebs were mechanically isolated by sweeping a cutting pipette beneath it, and subsequently patched with glass electrodes (resistance ~7 MΩ).

For sodium current recordings, pipettes were filled with a potassium gluconate-based internal solution containing (in mM): 130 K-gluconate, 1 $MgCl_2$, 11 EGTA, 1 $CaCl_2$, 1 KCl, 2 Mg-ATP, 0.3 Na-GTP, 10 HEPES (pH adjusted to 7.2, ~290 mOsm), supplemented with 2 mM TEA-Cl. The external ACSF solution was supplemented with 5 mM 4-Aminopydine (4-AP) and 200 µM $CdCl_2$ to block K^+ and Ca^{2+} currents, respectively.

Whole-cell voltage-clamp recordings were performed using a MultiClamp amplifier (Molecular Devices, 700B). Currents were filtered at 4 kHz (low-pass) and digitized at 20 kHz via a Digidata interface (Molecular Devices, 1440A). Series resistance was compensated by 80% to minimize voltage errors. Leak currents were subtracted by using an online P/4 procedure. The holding potential was set to -70 mV, approximating the resting membrane potential of cortical neurons. To assess sodium current density, a hyperpolarization prepulse to -110 mV (200 ms) was used to remove inactivation, followed by a 20-ms depolarization to 0 mV. Sodium current density (nA/pF) was calculated by normalizing peak current to bleb capacitance. To evaluate Nav channel slow inactivation a single 5-s depolarizing pulse (0 mV) was applied to induce slow inactivation followed by a test pulses (0 mV, 20 ms) separated by 10-ms recovery intervals at -70 mV. The fraction of available Nav channels was calculated by normalizing the peak current amplitude of each test pulse to the peak current measured at the onset of the 5-s depolarization.

Co-immunoprecipitation in transfected HEK293T cells

In co-immunoprecipitation experiments, one protein-of-interest was tagged with an HA epitope and the other with a Flag epitope. The pCAGIG vector bearing either a HA or Flag tag alone was used as a control in paired constructs. HEK293T cells transfected with a pair of constructs were harvested 24 hours post-transfection for protein expression. Cells were lysed in

ice-cold lysis buffer (20 mM Tris-HCl, 150 mM NaCl, 0.5% n-Dodecyl β-D-maltoside (DDM, Anatrace, D310), and protease inhibitor cocktail (Selleckchem, B14002)) with gentle agitation at 4 °C for 2 hours. Lysates were centrifuged at 20,000 x g for 20 minutes at 4 °C to remove insoluble debris. The supernatant was transferred to a fresh tube and kept on ice.

Protein concentration of supernatant was determined using a colorimetric bicinchoninic acid (BCA) assay (Beyotime, P0012S). For each immunoprecipitation (IP), 400 μg of proteins was incubated with 30 μL of anti-HA nanobody magnetic beads (AlfaLifeBio, KTSM1335) or anti-Flag magnetic beads (Bimake, B26102) at 4 °C with rotation for 1 hour. Beads were then separated with DynaMag spin and washed three times with wash buffer (20 mM Tris-HCl, 150 mM NaCl, 0.05% DDM). The captured proteins were eluted with 25 μL SDS-PAGE loading buffer containing 100 mM DTT, followed by heating at 45 °C for 10 min. Samples were stored at -20 °C prior to western blot analysis.

Co-immunoprecipitation in mouse brain tissues

Brain tissues (~100 mg per sample) were freshly dissected from wild-type or *Prrt2-V5* knock-in mice, and homogenized on ice using glass homogenizers in 1 mL of Tris-buffered saline (TBS, 20 mM Tris-HCl, 150 mM NaCl, protease inhibitor cocktail). The homogenates were centrifuged at 800 x g for 10 min at 4 °C to remove nuclei and cell debris. Supernatants were subjected to centrifugation at 40,000 x g for 45 minutes at 4 °C to isolate membrane fractions. The resulting membrane-enriched pellets were resuspended in TBS and solubilized in lysis buffer containing 0.3% DDM for 3 hours at 4 °C. Lysates were then cleared by centrifugation at 20,000 x g for 20 minutes at 4 °C. Protein concentration was measured via BCA assay. For each IP, ~200 μg of proteins was incubated with 30 μL of V5-Trap magnetic beads (Chromotek, v5tma-20) at 4 °C with rotation for 1.5 hours. Beads were washed three times with wash buffer (20 mM Tris-HCl, 150 mM NaCl, 0.15% DDM), and bound proteins were eluted with 25 μL SDS-PAGE loading buffer containing 100 mM DTT, followed by heating at 45 °C for 10 min. Eluates were kept at -20 °C until use in western blotting.

Western blotting

Protein samples were separated using 4-12% PAGE Gel (Nanjing ACE Biotechnology, ET15412L) in MES-SDS running buffer at 140 V for 60 minutes. Proteins were transferred onto polyvinylidene difluoride (PVDF) membranes at 300 mA for 2 hours at 4 °C. The PVDF

membranes were blocked in 5% nonfat milk in TBST (TBS with 0.1% Tween-20) for 1 hour at room temperature, followed by incubation with indicated primary antibodies overnight at 4 °C with gentle agitation.

After three washes in TBST, membranes were incubated with HRP-conjugated secondary antibodies for 2 hours at room temperature. Following another three washes, chemiluminescent substrate (TIANGEN Biotech, PA112) was applied, and signals were detected using a blot imaging system (Analytikjena, ChemStudio 815). Densitometric analysis of protein bands was performed using QuantityOne software (Biorad, Quantity One 1-D analysis, v4.6.2). The primary antibodies we used in western blotting were as follow: Anti-human PRRT2 (Atlas antibodies, HPA014447), Anti-Nav1.2 (Alomone Labs, ASC-002), Anti-Nav1.1 (Alomone Labs, ASC-001), Anti-HA-Tag (Cell signaling technology, 3724S), Anti-GAPDH-HRP (KangChen Bio-tech,KC-5G5), Anti-ATP1B2 (Abcam, ab185210), Anti-mouse PRRT2 (Wiiget Biotech, Rp3246) and Anti-β Actin-HRP (Cell signaling technology, 5125S).

Animal Surgery

Mice were anesthetized with isoflurane (RWD life science, R510-22-10), using 4% for induction and 2% for maintenance. Body temperature was maintained throughout the procedure with a heating pad. Meloxicam (5 mg/kg, subcutaneous) was administered preoperatively for analgesia.

After securing the mice in a stereotaxic frame (RWD life science, Model 68528), 0.25% bupivacaine was locally injected at the incision sites for perioperative analgesia, and ophthalmic ointment was applied to protect the cornea. A midline incision was made to expose the skull, which was cleaned with 2% hydrogen peroxide using sterile cotton swabs to remove connective tissue. The skull surface was leveled to a stereotaxic plane, and the bregma was identified and marked. Once dry, the exposed skull was coated with a light-curing self-etch adhesive (3M ESPE Single Bond Universal).

Two small craniotomies (~0.6 mm in diameter) were made over the left sensory cortex (anterior-posterior (AP) -0.8 mm; medial-lateral (ML) 1.5 mm) and visual cortex (AP -3.5 mm, ML 1.5 mm) for the insertion of bipolar stimulation electrodes (180 μm in diameter), which were implanted to a depth of -0.6 mm from the dura. Stainless steel screws were used as EEG electrodes: one was implanted into the right visual cortex (AP -2.25 mm, ML -1.5 mm), and

the second into the right cerebellar vermis to serve as the reference. An additional screw was placed in the left cerebellar hemisphere as the ground. The electrodes and a custom-made head plate were affixed to the skull using dental cement.

Post-operatively, meloxicam (5 mg/kg, subcutaneously) was administered once daily for 3 consecutive days. Mice were allowed to recover for one week prior to electrical stimulation and EEG recording.

Electrostimulation and EEG recording in the cerebral cortex

One week after surgery, mice were habituated to a custom-built head plate holder for 30 minutes per day over three consecutive days prior to testing.

For stimulation experiments, the pre-implanted electrodes were connected to a stimulus isolator (AMPI, ISO Flex). Electrical pulses (1 ms pulse width, 60 Hz frequency, 2 s duration) were delivered through the isolator and controlled via TTL signals from a pulse generator (RWD life science, R820). EEG signals (bandpass: 1-300 Hz) were amplified 1000-fold using an AC/DC differential amplifier (A-M Systems, Model 3000), digitized at 1 kHz with a Digidata (Molecular Devices, 1332A), and acquired using Clampex software (Molecular Devices, v10.7).

To assess cortical resilience in *Prrt2*-mutant versus wild-type mice, a stimulus-response protocol was employed using progressively increasing current intensities (0, 20, 40, 80, 120, 160, 200, 240, 280, 320 µA). Each stimulation was separated by a 24-hour interval. The stimulation threshold was defined as the lowest current intensity that induced after-discharges (lasting ≥ 2 seconds) in the EEG trace. Each EEG recording lasted for 5 minutes, with electrical stimulation delivered immediately following a 1-minute baseline period.

Statistics

All grouped data are presented as mean ± standard error of mean (s.e.m) unless otherwise stated. Statistical analyses were performed using Graphpad Prism 8 (GraphPad Software Inc, La Jolla, US). No statistical methods were used to pre-determine the sample sizes. The D'Agostino-Pearson omnibus (K2) test was used to assess normality.

Two-tailed, unpaired Student's *t*-tests were applied in Figures1B, 7B and 7D. A two-tailed, paired Student's *t*-test was used in Figures 6D-F and supplement 4B. Two-tailed, unpaired Mann-Whitney test was applied in Figure 7H. Two-way ANOVAs were conducted for comparisons in Figures 1D, 1F-G, 2B-C, 2E-F, 3C-D, 3F-G, 4B-D, 4F-H, 7I, supplement 1B, supple-

ment 2C-D, and supplement 3B-C. If necessary, the Gessier-Greenhouse correction was applied to adjust for violations of sphericity.

Statistical tests and sample sizes (including number of cells, slices, or animals) are stated in the figure legends. No data were excluded from analyses. Asterisks in figures denote significance levels: *P□<□0.05, **P□<□0.01, ***P□<□0.001, ****P□<□0.0001, n.s., not significant.

Co-immunoprecipitation assays were independently repeated at least three times in both *in vitro* and *in vivo* tests. All attempts at replicating experiments presented in the manuscript have obtained consistent conclusions.

Electrophysiological recordings were conducted with the experimenter blinded to group identity (transfected condition or animal genotype).

Acknowledgements

The authors thank Fei Dong, Ting-Bin Ma, Xi-Zhou, Wen-Zhang, Wei-Ke, Yue-Jie Xiao and Xue-Qin Jin for technical support for electrophysiological recording. We thank Huai-Zong Shen, Zhang-Qiang Li, Xue-Jing Li and Shu-Jia Zhu for experimental support for protein expression. We thank Tong-Zhou Li, Hong-Zhang, Jun-Jun Liu and Hai-Yan Zhen from ICE Bioscience for experimental support in sodium current recording. We appreciate the staff at the Core Facilities for their generous technical support, and members of Xiong Lab for technical support and insightful discussions.

This work was supported by National Natural Science Foundation of China, grants 82271269 (B.L.) and 82021001 (Z.-Q.X.); Innovation of Science and Technology 2030-Major Project “platform of nonhuman primate models", grant 2021ZD0200900 (Z.-Q.X.); and Shanghai Municipal Science and Technology Major Project (Z.-Q.X.).

Additional information

Materials availability

All plasmids and mice generated in this study are available from the lead contact with a completed materials transfer agreement.

Data and code availability

The data supporting the findings of this study are included in the main text. This paper does not report the original code.

Contributions

Z.-Q.X. and B.L. conceived the study and designed the experiments. B.L., Q.-W.X. and J.Z. carried out cellular and molecular experiments and data analyses. X.-M.W. and J.-Y.H. performed animal experiments and data analyses. L.Z., J.Z. and K.-X.L. are responsible for plasmids construction. G.Y. was responsible for the knock-in mice generation. Y.-X.Z. helped with animal surgery and behavior analyses. B.L. wrote the manuscript. Q.-W.X., J.Z., X.-M.W. and J.-Y.H. carried out manuscript review and editing. Z.-Q.X. and B.L. carried out project supervision, data interpretation and funding acquisition.

Competing interests

The authors declare no competing interests.

Supplemental information

Figures supplement 1-4.

References

Abramson, J., Adler, J., Dunger, J., Evans, R., Green, T., Pritzel, A., . . . Jumper, J. M. (2024). Accurate structure prediction of biomolecular interactions with AlphaFold 3. *Nature, 630*(8016), 493-500. doi:10.1038/s41586-024-07487-w

Armstrong, C. M., & Bezanilla, F. (1977). Inactivation of the sodium channel. II. Gating current experiments. *J Gen Physiol, 70*(5), 567-590. doi:10.1085/jgp.70.5.567

Balser, J. R., Nuss, H. B., Chiamvimonvat, N., Perez-Garcia, M. T., Marban, E., & Tomaselli, G. F. (1996). External pore residue mediates slow inactivation in mu 1 rat skeletal muscle sodium channels. *J Physiol, 494 (Pt 2)*(Pt 2), 431-442. doi:10.1113/jphysiol.1996.sp021503

Bar-Yehuda, D., & Korngreen, A. (2008). Space-clamp problems when voltage clamping neurons expressing voltage-gated conductances. *J Neurophysiol, 99*(3), 1127-1136. doi:10.1152/jn.01232.2007

Bendahhou, S., Cummins, T. R., Kula, R. W., Fu, Y. H., & Ptacek, L. J. (2002). Impairment of slow inactivation as a common mechanism for periodic paralysis in DIIS4-S5. *Neurology, 58*(8), 1266-1272. doi:10.1212/wnl.58.8.1266

Bett, G. C., Dinga-Madou, I., Zhou, Q., Bondarenko, V. E., & Rasmusson, R. L. (2011). A model of the interaction between N-type and C-type inactivation in Kv1.4 channels. *Biophys J, 100*(1), 11-21. doi:10.1016/j.bpj.2010.11.011

Bezanilla, F., & Armstrong, C. M. (1977). Inactivation of the sodium channel. I. Sodium current experiments. *J Gen Physiol, 70*(5), 549-566. doi:10.1085/jgp.70.5.549

Binda, F., Valente, P., Marte, A., Baldelli, P., & Benfenati, F. (2021). Increased responsiveness at the cerebellar input stage in the PRRT2 knockout model of paroxysmal kinesigenic dyskinesia. *Neurobiol Dis, 152*, 105275. doi:10.1016/j.nbd.2021.105275

Blume, W. T., Jones, D. C., & Pathak, P. (2004). Properties of after-discharges from cortical electrical stimulation in focal epilepsies. *Clin Neurophysiol, 115*(4), 982-989. doi:10.1016/j.clinph.2003.11.023

Cannon, S. C. (2018). Sodium Channelopathies of Skeletal Muscle. *Handb Exp Pharmacol, 246*, 309-330. doi:10.1007/164_2017_52

Catterall, W. A. (2023). Voltage gated sodium and calcium channels: Discovery, structure, function, and Pharmacology. *Channels (Austin), 17*(1), 2281714. doi:10.1080/19336950.2023.2281714

Catterall, W. A., Goldin, A. L., & Waxman, S. G. (2005). International Union of Pharmacology. XLVII. Nomenclature and structure-function relationships of voltage-gated sodium channels. *Pharmacol Rev, 57*(4), 397-409. doi:10.1124/pr.57.4.4

Catterall, W. A., Wisedchaisri, G., & Zheng, N. (2020). The conformational cycle of a prototypical voltage-gated sodium channel. *Nat Chem Biol, 16*(12), 1314-1320. doi:10.1038/s41589-020-0644-4

Chancey, J. H., Shockett, P. E., & O'Reilly, J. P. (2007). Relative resistance to slow inactivation of human cardiac Na+ channel hNav1.5 is reversed by lysine or glutamine substitution at V930 in D2-S6. *Am J Physiol Cell Physiol, 293*(6), C1895-1905. doi:10.1152/ajpcell.00377.2007

Chatterjee, S., Vyas, R., Chalamalasetti, S. V., Sahu, I. D., Clatot, J., Wan, X., . . . Chakrapani, S. (2018). The voltage-gated sodium channel pore exhibits conformational flexibility during slow inactivation. *J Gen Physiol, 150*(9), 1333-1347. doi:10.1085/jgp.201812118

Chen, W. J., Lin, Y., Xiong, Z. Q., Wei, W., Ni, W., Tan, G. H., . . . Wu, Z. Y. (2011). Exome sequencing identifies truncating mutations in PRRT2 that cause paroxysmal kinesigenic dyskinesia. *Nat Genet, 43*(12), 1252-1255. doi:10.1038/ng.1008

Chen, Y., Yu, F. H., Surmeier, D. J., Scheuer, T., & Catterall, W. A. (2006). Neuromodulation of Na+ channel slow inactivation via cAMP-dependent protein kinase and protein kinase C. *Neuron, 49*(3), 409-420. doi:10.1016/j.neuron.2006.01.009

Cummins, T. R., & Sigworth, F. J. (1996). Impaired slow inactivation in mutant sodium channels. *Biophys J, 71*(1), 227-236. doi:10.1016/S0006-3495(96)79219-6

Cusdin, F. S., Clare, J. J., & Jackson, A. P. (2008). Trafficking and cellular distribution of voltage-gated sodium channels. *Traffic, 9*(1), 17-26. doi:10.1111/j.1600-0854.2007.00673.x

Dib-Hajj, S. D., Geha, P., & Waxman, S. G. (2017). Sodium channels in pain disorders: pathophysiology and prospects for treatment. *Pain, 158 Suppl 1*(Suppl 1), S97-S107. doi:10.1097/j.pain.0000000000000854

Dover, K., Solinas, S., D'Angelo, E., & Goldfarb, M. (2010). Long-term inactivation particle for voltage-gated sodium channels. *J Physiol, 588*(Pt 19), 3695-3711. doi:10.1113/jphysiol.2010.192559

Ehrlich, K. C., Lacey, M., & Ehrlich, M. (2020). Epigenetics of Skeletal Muscle-Associated Genes in the ASB, LRRC, TMEM, and OSBPL Gene Families. *Epigenomes, 4*(1). doi:10.3390/epigenomes4010001

Escayg, A., & Goldin, A. L. (2010). Sodium channel SCN1A and epilepsy: mutations and mechanisms. *Epilepsia, 51*(9), 1650-1658. doi:10.1111/j.1528-1167.2010.02640.x

Featherstone, D. E., Richmond, J. E., & Ruben, P. C. (1996). Interaction between fast and slow inactivation in Skm1 sodium channels. *Biophys J, 71*(6), 3098-3109. doi:10.1016/S0006-3495(96)79504-8

Franchi, F., Marte, A., Corradi, B., Sterlini, B., Alberini, G., Romei, A., . . . Benfenati, F. (2023). The intramembrane COOH-terminal domain of PRRT2 regulates voltage-dependent Na(+) channels. *J Biol Chem,* 104632. doi:10.1016/j.jbc.2023.104632

Fruscione, F., Valente, P., Sterlini, B., Romei, A., Baldassari, S., Fadda, M., . . . Benfenati, F. (2018). PRRT2 controls neuronal excitability by negatively modulating Na^+ channel 1.2/1.6 activity.

Brain, 141(4), 1000-1016. doi:10.1093/brain/awy051

Gade, A. R., Marx, S. O., & Pitt, G. S. (2020). An interaction between the III-IV linker and CTD in NaV1.5 confers regulation of inactivation by CaM and FHF. *J Gen Physiol, 152*(2). doi:10.1085/jgp.201912434

Ganguly, S., Thompson, C. H., & George, A. L., Jr. (2021). Enhanced slow inactivation contributes to dysfunction of a recurrent SCN2A mutation associated with developmental and epileptic encephalopathy. *J Physiol, 599*(18), 4375-4388. doi:10.1113/JP281834

Ghovanloo, M. R., Effraim, P. R., Yuan, J. H., Schulman, B. R., Jacobs, D. S., Dib-Hajj, S. D., & Waxman, S. G. (2023). Nav1.7 P610T mutation in two siblings with persistent ocular pain after corneal axon transection: impaired slow inactivation and hyperexcitable trigeminal neurons. *J Neurophysiol, 129*(3), 609-618. doi:10.1152/jn.00457.2022

Goetz, R., Dover, K., Laezza, F., Shtraizent, N., Huang, X., Tchetchik, D., . . . Mohammadi, M. (2009). Crystal structure of a fibroblast growth factor homologous factor (FHF) defines a conserved surface on FHFs for binding and modulation of voltage-gated sodium channels. *J Biol Chem, 284*(26), 17883-17896. doi:10.1074/jbc.M109.001842

Goldin, A. L. (2001). Resurgence of sodium channel research. *Annu Rev Physiol, 63*, 871-894. doi:10.1146/annurev.physiol.63.1.871

Goldin, A. L. (2003). Mechanisms of sodium channel inactivation. *Curr Opin Neurobiol, 13*(3), 284-290. doi:10.1016/s0959-4388(03)00065-5

Hayward, L. J., Sandoval, G. M., & Cannon, S. C. (1999). Defective slow inactivation of sodium channels contributes to familial periodic paralysis. *Neurology, 52*(7), 1447-1453. doi:10.1212/wnl.52.7.1447

He, B., & Soderlund, D. M. (2014). Functional expression of Rat Nav1.6 voltage-gated sodium channels in HEK293 cells: modulation by the auxiliary beta1 subunit. *PLoS One, 9*(1), e85188. doi:10.1371/journal.pone.0085188

Hedrich, U. B. S., Lauxmann, S., & Lerche, H. (2019). SCN2A channelopathies: Mechanisms and models. *Epilepsia, 60 Suppl 3*, S68-S76. doi:10.1111/epi.14731

Hodgkin, A. L., & Huxley, A. F. (1952). A quantitative description of membrane current and its application to conduction and excitation in nerve. *J Physiol, 117*(4), 500-544. doi:10.1113/jphysiol.1952.sp004764

Hoshi, T., Zagotta, W. N., & Aldrich, R. W. (1990). Biophysical and molecular mechanisms of Shaker potassium channel inactivation. *Science, 250*(4980), 533-538. doi:10.1126/science.2122519

Hu, W., & Shu, Y. (2012). Axonal bleb recording. *Neurosci Bull, 28*(4), 342-350. doi:10.1007/s12264-012-1247-1

Isom, L. L., De Jongh, K. S., Patton, D. E., Reber, B. F., Offord, J., Charbonneau, H., . . . Catterall, W. A. (1992). Primary structure and functional expression of the beta 1 subunit of the rat brain sodium channel. *Science, 256*(5058), 839-842. doi:10.1126/science.1375395

Jiang, D., Shi, H., Tonggu, L., Gamal El-Din, T. M., Lenaeus, M. J., Zhao, Y., . . . Catterall, W. A. (2020). Structure of the Cardiac Sodium Channel. *Cell, 180*(1), 122-134 e110. doi:10.1016/j.cell.2019.11.041

Lee, H. Y., Huang, Y., Bruneau, N., Roll, P., Roberson, E. D., Hermann, M., . . . Ptacek, L. J. (2012). Mutations in the gene PRRT2 cause paroxysmal kinesigenic dyskinesia with infantile convulsions. *Cell Rep, 1*(1), 2-12. doi:10.1016/j.celrep.2011.11.001

Lu, B., Lou, S. S., Xu, R. S., Kong, D. L., Wu, R. J., Zhang, J., . . . Xiong, Z. Q. (2021). Cerebellar spreading

844 depolarization mediates paroxysmal movement disorder. *Cell Rep, 36*(12), 109743.
845 doi:10.1016/j.celrep.2021.109743
846 Makita, N., Bennett, P. B., & George, A. L., Jr. (1996). Molecular determinants of beta 1 subunit-
847 induced gating modulation in voltage-dependent Na+ channels. *J Neurosci, 16*(22), 7117-
848 7127. doi:10.1523/JNEUROSCI.16-22-07117.1996
849 Mantegazza, M., Cestele, S., & Catterall, W. A. (2021). Sodium channelopathies of skeletal muscle and
850 brain. *Physiol Rev, 101*(4), 1633-1689. doi:10.1152/physrev.00025.2020
851 Matsuda, T., & Cepko, C. L. (2004). Electroporation and RNA interference in the rodent retina in vivo
852 and in vitro. *Proc Natl Acad Sci U S A, 101*(1), 16-22. doi:10.1073/pnas.2235688100
853 Meisler, M. H., Hill, S. F., & Yu, W. (2021). Sodium channelopathies in neurodevelopmental disorders.
854 *Nat Rev Neurosci, 22*(3), 152-166. doi:10.1038/s41583-020-00418-4
855 Misra, S. N., Kahlig, K. M., & George, A. L., Jr. (2008). Impaired NaV1.2 function and reduced cell
856 surface expression in benign familial neonatal-infantile seizures. *Epilepsia, 49*(9), 1535-1545.
857 doi:10.1111/j.1528-1167.2008.01619.x
858 Mitrovic, N., George, A. L., Jr., & Horn, R. (2000). Role of domain 4 in sodium channel slow inactivation.
859 *J Gen Physiol, 115*(6), 707-718. doi:10.1085/jgp.115.6.707
860 Noreng, S., Li, T., & Payandeh, J. (2021). Structural Pharmacology of Voltage-Gated Sodium Channels. *J*
861 *Mol Biol, 433*(17), 166967. doi:10.1016/j.jmb.2021.166967
862 Olsen, S. K., Garbi, M., Zampieri, N., Eliseenkova, A. V., Ornitz, D. M., Goldfarb, M., & Mohammadi, M.
863 (2003). Fibroblast growth factor (FGF) homologous factors share structural but not functional
864 homology with FGFs. *J Biol Chem, 278*(36), 34226-34236. doi:10.1074/jbc.M303183200
865 Oort, P. J., Warden, C. H., Baumann, T. K., Knotts, T. A., & Adams, S. H. (2007). Characterization of
866 Tusc5, an adipocyte gene co-expressed in peripheral neurons. *Mol Cell Endocrinol, 276*(1-2),
867 24-35. doi:10.1016/j.mce.2007.06.005
868 Pan, X., Li, Z., Huang, X., Huang, G., Gao, S., Shen, H., . . . Yan, N. (2019). Molecular basis for pore
869 blockade of human Na(+) channel Na(v)1.2 by the mu-conotoxin KIIIA. *Science, 363*(6433),
870 1309-1313. doi:10.1126/science.aaw2999
871 Pan, X., Li, Z., Jin, X., Zhao, Y., Huang, G., Huang, X., . . . Yan, N. (2021). Comparative structural analysis
872 of human Na(v)1.1 and Na(v)1.5 reveals mutational hotspots for sodium channelopathies.
873 *Proc Natl Acad Sci U S A, 118*(11). doi:10.1073/pnas.2100066118
874 Payandeh, J. (2018). Progress in understanding slow inactivation speeds up. *J Gen Physiol, 150*(9),
875 1235-1238. doi:10.1085/jgp.201812149
876 Remme, C. A. (2013). Cardiac sodium channelopathy associated with SCN5A mutations:
877 electrophysiological, molecular and genetic aspects. *J Physiol, 591*(17), 4099-4116.
878 doi:10.1113/jphysiol.2013.256461
879 Riant, F., Roos, C., Roubertie, A., Barbance, C., Hadjadj, J., Auvin, S., . . . Ducros, A. (2022). Hemiplegic
880 Migraine Associated With PRRT2 Variations: A Clinical and Genetic Study. *Neurology, 98*(1),
881 e51-e61. doi:10.1212/WNL.0000000000012947
882 Richmond, J. E., Featherstone, D. E., Hartmann, H. A., & Ruben, P. C. (1998). Slow inactivation in
883 human cardiac sodium channels. *Biophys J, 74*(6), 2945-2952. doi:10.1016/S0006-
884 3495(98)78001-4
885 Rudy, B. (1978). Slow inactivation of the sodium conductance in squid giant axons. Pronase resistance.
886 *J Physiol, 283*, 1-21. doi:10.1113/jphysiol.1978.sp012485
887 Sallman Almen, M., Bringeland, N., Fredriksson, R., & Schioth, H. B. (2012). The dispanins: a novel

gene family of ancient origin that contains 14 human members. *PLoS One, 7*(2), e31961. doi:10.1371/journal.pone.0031961

Santana-Varela, S., Bogdanov, Y. D., Gossage, S. J., Okorokov, A. L., Li, S., de Clauser, L., . . . Cox, J. J. (2021). Tools for analysis and conditional deletion of subsets of sensory neurons. *Wellcome Open Res, 6*, 250. doi:10.12688/wellcomeopenres.17090.1

Shibata, T., Koide, H., Hayashi, R., Nagata, K., Takeo, C., Yoshida, T., . . . Tatsuno, I. (2007). Molecular cloning and characterization of rat brain endothelial cell derived gene-1 (tumor suppressor candidate 5) expressing abundantly in adipose tissues. *Mol Cell Endocrinol, 263*(1-2), 38-45. doi:10.1016/j.mce.2006.08.007

Silva, J. (2014). Slow inactivation of Na(+) channels. *Handb Exp Pharmacol, 221*, 33-49. doi:10.1007/978-3-642-41588-3_3

Tan, G. H., Liu, Y. Y., Wang, L., Li, K., Zhang, Z. Q., Li, H. F., . . . Xiong, Z. Q. (2018). PRRT2 deficiency induces paroxysmal kinesigenic dyskinesia by regulating synaptic transmission in cerebellum. *Cell Res, 28*(1), 90-110. doi:10.1038/cr.2017.128

Thompson, C. H., Potet, F., Abramova, T. V., DeKeyser, J. M., Ghabra, N. F., Vanoye, C. G., . . . George, A. L. (2023). Epilepsy-associated SCN2A (NaV1.2) variants exhibit diverse and complex functional properties. *J Gen Physiol, 155*(10). doi:10.1085/jgp.202313375

Todt, H., Dudley, S. C., Jr., Kyle, J. W., French, R. J., & Fozzard, H. A. (1999). Ultra-slow inactivation in mu1 Na+ channels is produced by a structural rearrangement of the outer vestibule. *Biophys J, 76*(3), 1335-1345. doi:10.1016/S0006-3495(99)77296-6

Ulbricht, W. (1977). Ionic channels and gating currents in excitable membranes. *Annu Rev Biophys Bioeng, 6*, 7-31. doi:10.1146/annurev.bb.06.060177.000255

Valente, P., Marte, A., Franchi, F., Sterlini, B., Casagrande, S., Corradi, A., . . . Benfenati, F. (2023). A Push-Pull Mechanism Between PRRT2 and beta4-subunit Differentially Regulates Membrane Exposure and Biophysical Properties of NaV1.2 Sodium Channels. *Mol Neurobiol, 60*(3), 1281-1296. doi:10.1007/s12035-022-03112-x

Venkatesan, K., Liu, Y., & Goldfarb, M. (2014). Fast-onset long-term open-state block of sodium channels by A-type FHFs mediates classical spike accommodation in hippocampal pyramidal neurons. *J Neurosci, 34*(48), 16126-16139. doi:10.1523/JNEUROSCI.1271-14.2014

Vilin, Y. Y., Makita, N., George, A. L., Jr., & Ruben, P. C. (1999). Structural determinants of slow inactivation in human cardiac and skeletal muscle sodium channels. *Biophys J, 77*(3), 1384-1393. doi:10.1016/S0006-3495(99)76987-0

Vilin, Y. Y., & Ruben, P. C. (2001). Slow inactivation in voltage-gated sodium channels: molecular substrates and contributions to channelopathies. *Cell Biochem Biophys, 35*(2), 171-190. doi:10.1385/CBB:35:2:171

Wallner, M., Weigl, L., Meera, P., & Lotan, I. (1993). Modulation of the skeletal muscle sodium channel alpha-subunit by the beta 1-subunit. *FEBS Lett, 336*(3), 535-539. doi:10.1016/0014-5793(93)80871-q

Wang, D. W., Makita, N., Kitabatake, A., Balser, J. R., & George, A. L., Jr. (2000). Enhanced Na(+) channel intermediate inactivation in Brugada syndrome. *Circ Res, 87*(8), E37-43. doi:10.1161/01.res.87.8.e37

Wang, J. L., Cao, L., Li, X. H., Hu, Z. M., Li, J. D., Zhang, J. G., . . . Tang, B. S. (2011). Identification of PRRT2 as the causative gene of paroxysmal kinesigenic dyskinesias. *Brain, 134*(Pt 12), 3493-3501. doi:10.1093/brain/awr289

932 Wang, S. Y., & Wang, G. K. (1997). A mutation in segment I-S6 alters slow inactivation of sodium
933 channels. *Biophys J, 72*(4), 1633-1640. doi:10.1016/S0006-3495(97)78809-X
934 Waxman, S. G. (2013). Painful Na-channelopathies: an expanding universe. *Trends Mol Med, 19*(7),
935 406-409. doi:10.1016/j.molmed.2013.04.003
936 Webb, J., Wu, F. F., & Cannon, S. C. (2009). Slow inactivation of the NaV1.4 sodium channel in
937 mammalian cells is impeded by co-expression of the beta1 subunit. *Pflugers Arch, 457*(6),
938 1253-1263. doi:10.1007/s00424-008-0600-8
939 Wisedchaisri, G., & Gamal El-Din, T. M. (2022). Druggability of Voltage-Gated Sodium Channels-
940 Exploring Old and New Drug Receptor Sites. *Front Pharmacol, 13*, 858348.
941 doi:10.3389/fphar.2022.858348
942 Xiong, W., Farukhi, Y. Z., Tian, Y., Disilvestre, D., Li, R. A., & Tomaselli, G. F. (2006). A conserved ring of
943 charge in mammalian Na+ channels: a molecular regulator of the outer pore conformation
944 during slow inactivation. *J Physiol, 576*(Pt 3), 739-754. doi:10.1113/jphysiol.2006.115105
945 Xu, R., Thomas, E. A., Gazina, E. V., Richards, K. L., Quick, M., Wallace, R. H., . . . Petrou, S. (2007).
946 Generalized epilepsy with febrile seizures plus-associated sodium channel beta1 subunit
947 mutations severely reduce beta subunit-mediated modulation of sodium channel function.
948 *Neuroscience, 148*(1), 164-174. doi:10.1016/j.neuroscience.2007.05.038
949 Yamano, R., Miyazaki, H., & Nukina, N. (2022). The diffuse distribution of Nav1.2 on mid-axonal
950 regions is a marker for unmyelinated fibers in the central nervous system. *Neurosci Res, 177*,
951 145-150. doi:10.1016/j.neures.2021.11.005
952 Yang, H., Wang, H., & Jaenisch, R. (2014). Generating genetically modified mice using CRISPR/Cas-
953 mediated genome engineering. *Nat Protoc, 9*(8), 1956-1968. doi:10.1038/nprot.2014.134
954 Yu, F. H., Mantegazza, M., Westenbroek, R. E., Robbins, C. A., Kalume, F., Burton, K. A., . . . Catterall, W.
955 A. (2006). Reduced sodium current in GABAergic interneurons in a mouse model of severe
956 myoclonic epilepsy in infancy. *Nat Neurosci, 9*(9), 1142-1149. doi:10.1038/nn1754
957 Zang, Y., Marder, E., & Marom, S. (2023). Sodium channel slow inactivation normalizes firing in axons
958 with uneven conductance distributions. *Curr Biol, 33*(9), 1818-1824 e1813.
959 doi:10.1016/j.cub.2023.03.043
960
961

Figures

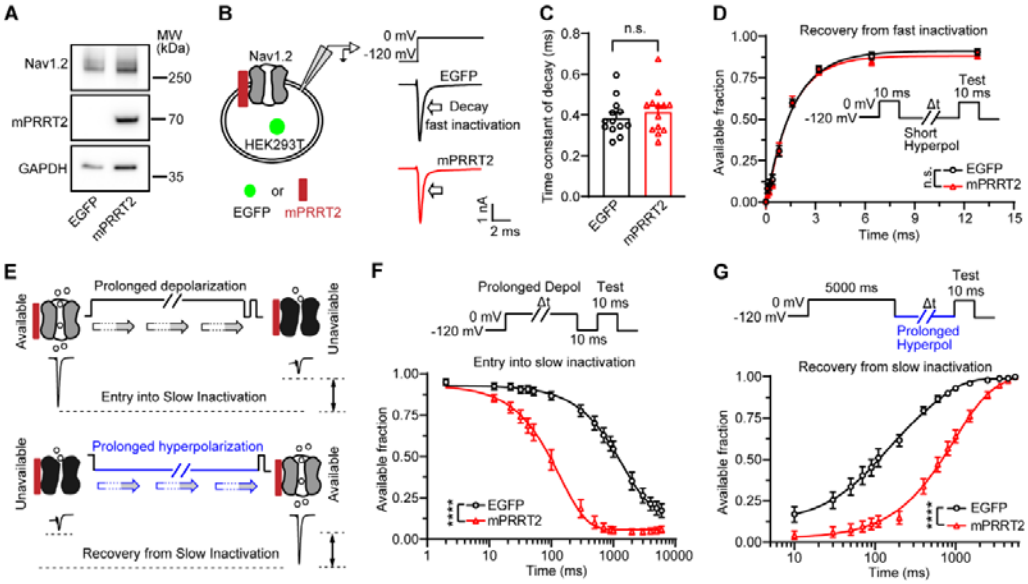

Figure 1 PRRT2 regulates slow inactivation of Nav1.2 channels

(A) Representative immunoblots showing PRRT2 protein expression in Nav1.2-stably expressing HEK293T cells transfected with constructs encoding either EGFP or mouse PRRT2 (mPRRT2). MW, molecular weight.

(B) Schematic of whole-cell recording (left) and representative traces of sodium currents evoked by a brief depolarization (right). The arrow indicate sodium current decay due to fast inactivation. Scale bar, 1 nA by 2 ms.

(C) Decay time constants of sodium currents in response to 20-ms depolarization (EGFP: n = 13 cells, mPRRT2: n = 13 cells).

(D) Recovery from fast inactivation of Nav1.2 channels (EGFP: n = 10 cells, mPRRT2: n = 7 cells). Insert: Protocol for examining fast inactivation recovery.

(E) Schematic diagram of entry into and recover from slow inactivation of voltage-gated sodium channels. Slow inactivation modulates the availability of the sodium channels.

(F) Entry into slow-inactivated state of Nav1.2 channels induced by progressive longer depolarization (EGFP: n = 6 cells, mPRRT2: n = 6 cells).

(G) The effects of PRRT2 on the recovery of Nav1.2 channels from slow-inactivated state induced by 5-s depolarization (EGFP: n = 6 cells, PRRT2: n = 6 cells). Data were presented as mean ± s.e.m. Two-tailed, unpaired Student's t-test was used in C, and two-way ANOVAs were used in D, F, and G. ****P < 0.0001. n.s.,not significant.

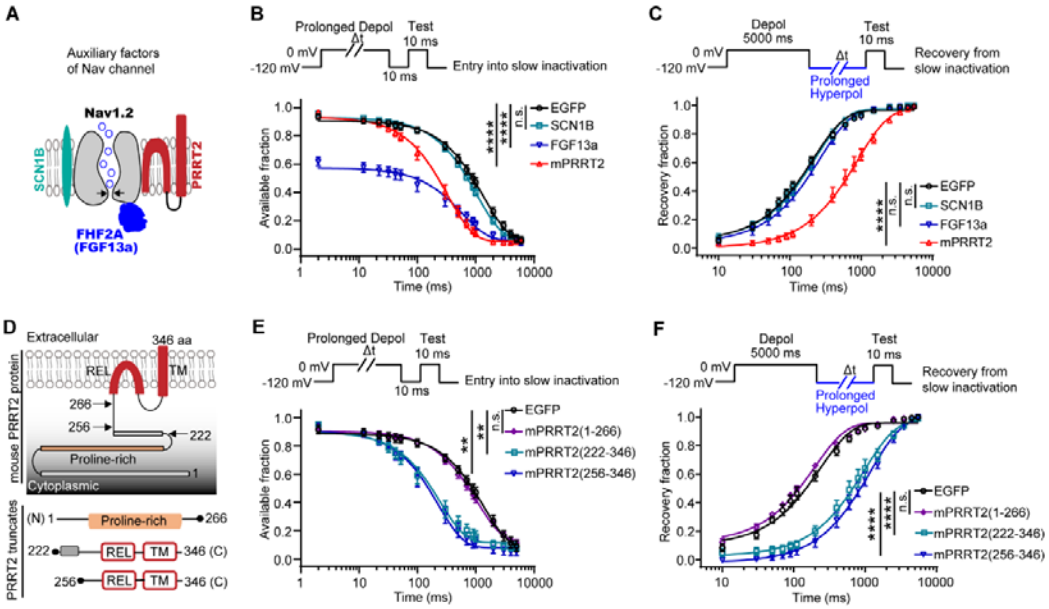

983

984 **Figure 2 Functional auxiliary factors in the regulation of Nav channel slow inactivation**

985 **(A)** Diagram of Nav channel with potent auxiliary factors, encompassing SCN1B, FHF2A (also
986 known as FGF13a) and PRRT2.

987 **(B)** The effects of auxiliary factors on the entry of Nav1.2 channels into slow inactivation
988 (EGFP: *n* = 12 cells, mPRRT2: *n* = 14 cells, SCN1B: *n* = 9 cells, FGF13a: *n* = 12 cells).

989 **(C)** The effects of auxiliary factors on the recovery of Nav1.2 channels from slow-inactivated
990 state induced by 5-s depolarization (EGFP: *n* = 12 cells, mPRRT2: *n* = 12 cells, SCN1B: *n* =
991 12 cells, FGF13a: *n* = 12 cells).

992 **(D)** Schematic representation of the putative topology of mouse PRRT2 and three truncates.
993 Numbers indicate the positions of the amino acid. REL, re-entrant loop. TM, transmembrane
994 domain. N, amino terminus. C, carboxyl terminus. aa, amino acid.

995 **(E)** The effects of PRRT2 truncates on the entry of Nav1.2 channels into slow inactivation
996 (EGFP: *n* = 5 cells, mPRRT2(1–266): *n* = 14 cells, mPRRT2(222–346): *n* = 12 cells,
997 mPRRT2(256–346): *n* = 12 cells).

998 **(F)** The effects of PRRT2 truncates on the recovery of Nav1.2 channels from slow-inactivated
999 state induced by 5-s depolarization (EGFP: *n* = 5 cells, mPRRT2(1–266): *n* = 10 cells,
1000 mPRRT2(222–346): *n* = 10 cells, mPRRT2(256–346): *n* = 12 cells). Data were presented as
1001 mean ± s.e.m. The main effect of group was assessed using two-way ANOVAs (B, C, E and
1002 F). $^{**}P < 0.01$, $^{****}P < 0.0001$, n.s., not significant.

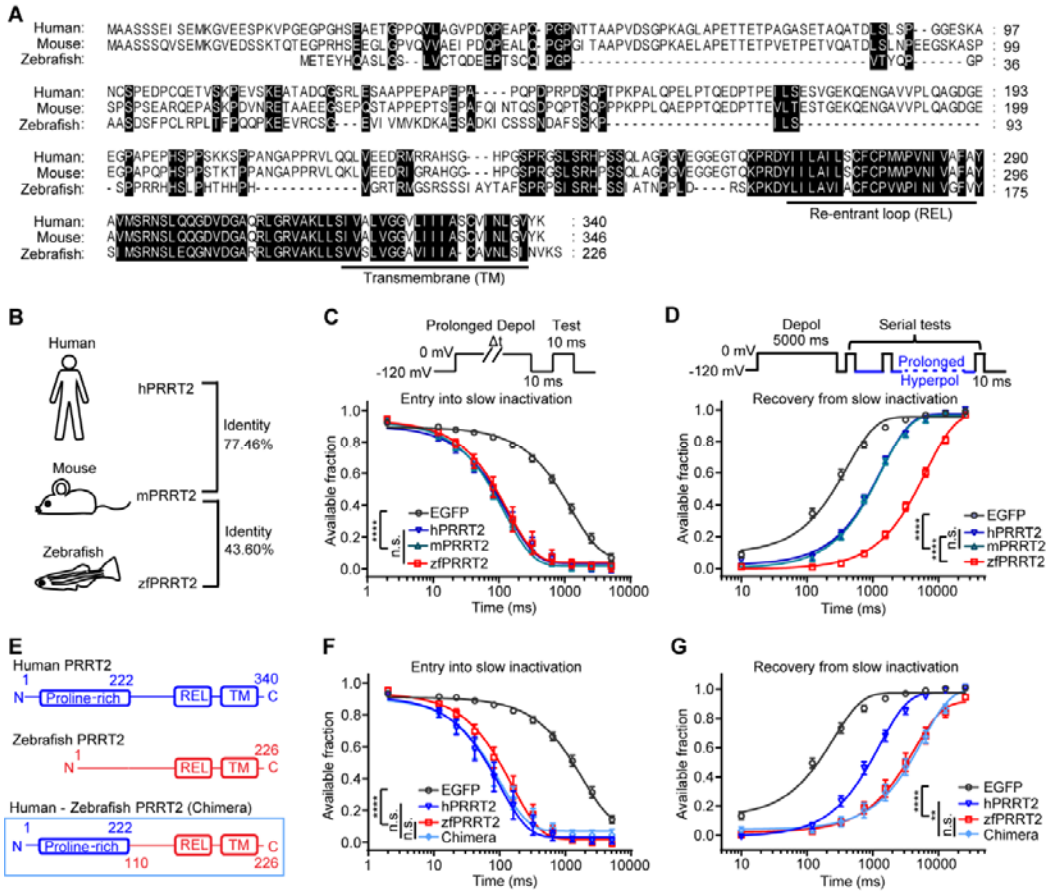

Figure 3 Evolutionarily conserved effects of PRRT2 on Nav channel slow inactivation

(A) Sequence alignment of PRRT2 protein in human, mouse and zebrafish. Conserved amino acids are highlighted and the membrane-associated domains in carboxyl terminus of PRRT2 are underlined. REL, re-entrant loop. TM, transmembrane domain.

(B) Sequence identity of PRRT2 protein in human (hPRRT2), mouse (mPRRT2) and zebrafish (zfPRRT2). Identity is calculated by using protein BLAST tool from NCBI.

(C) The effects of PRRT2 from different species on the entry of Nav1.2 channels into slow inactivation (EGFP: *n* = 16 cells, mPRRT2: *n* = 19 cells, hPRRT2: *n* = 20 cells, zfPRRT2: *n* = 11 cells).

(D) The effects of PRRT2 from different species on the recovery of Nav1.2 channels from slow-inactivated state induced by 5-s depolarization (EGFP: *n* = 16 cells, mPRRT2: *n* = 19 cells, hPRRT2: *n* = 19 cells, zfPRRT2: *n* = 11 cells).

(E) Diagram for the chimeric construct of PRRT2 originated from human and zebrafish.

(F) The effect of chimeric PRRT2 on the entry of Nav1.2 channels into slow inactivation

(EGFP: n = 11 cells, hPRRT2: n = 6 cells, zfPRRT2: n = 10 cells, Chimera: n = 11 cells). **(G)** The effect of Chimeric PRRT2 on the recovery of Nav1.2 channels from slow-inactivated state induced by 5-s depolarization (EGFP: n = 11 cells, hPRRT2: n = 6 cells, zfPRRT2: n = 10 cells, Chimera: n = 9 cells). Data were presented as mean ± s.e.m. The main effect of group was assessed using two-way ANOVAs (C, D, F and G). **P < 0.01, ****P < 0.0001, n.s., not significant.

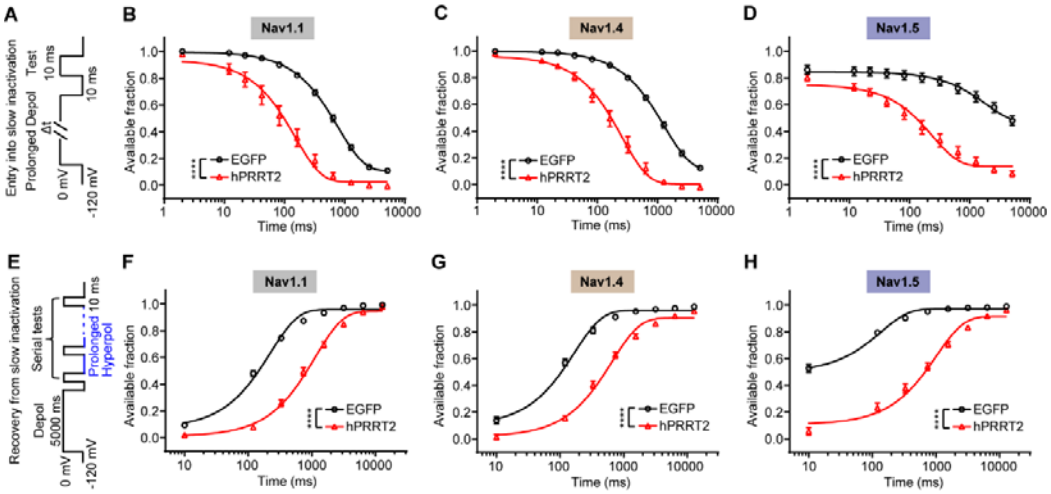

Figure 4 Uniform influence of PRRT2 on slow inactivation across human Nav isoforms

(A) Protocol for examining the entry of Nav channels into slow-inactivated state.

(B-D) The effects of human PRRT2 (hPRRT2) on the entry of Nav1.1, Nav1.4 and Nav1.5 channels into slow inactivation. In (B), analyses for Nav1.1 (EGFP: *n* = 10 cells, hPRRT2: *n* = 12 cells); In (C), analyses for Nav1.4 (EGFP: *n* = 11 cells, hPRRT2: *n* = 11 cells); In (D), analyses for Nav1.5 (EGFP: *n* = 17 cells, hPRRT2: *n* = 17 cells).

(E) Protocol for examining the recovery of Nav channels from slow-inactivated state.

(F-H) The effects of human PRRT2 on the recovery of Nav1.1, Nav1.4 and Nav1.5 channels from slow-inactivated state induced by 5-s depolarization. In (F), analyses for Nav1.1 (EGFP: *n* = 10 cells, hPRRT2: *n* = 12 cells); In (G), analyses for Nav1.4 (EGFP: *n* = 11 cells, hPRRT2: *n* = 11 cells); In (H), analyses for Nav1.5 (EGFP: *n* = 16 cells, hPRRT2: *n* = 15 cells).

Data were presented as mean ± s.e.m. The main effect of group was assessed using two-way ANOVAs (B-D and F-H). ****$P < 0.0001$.

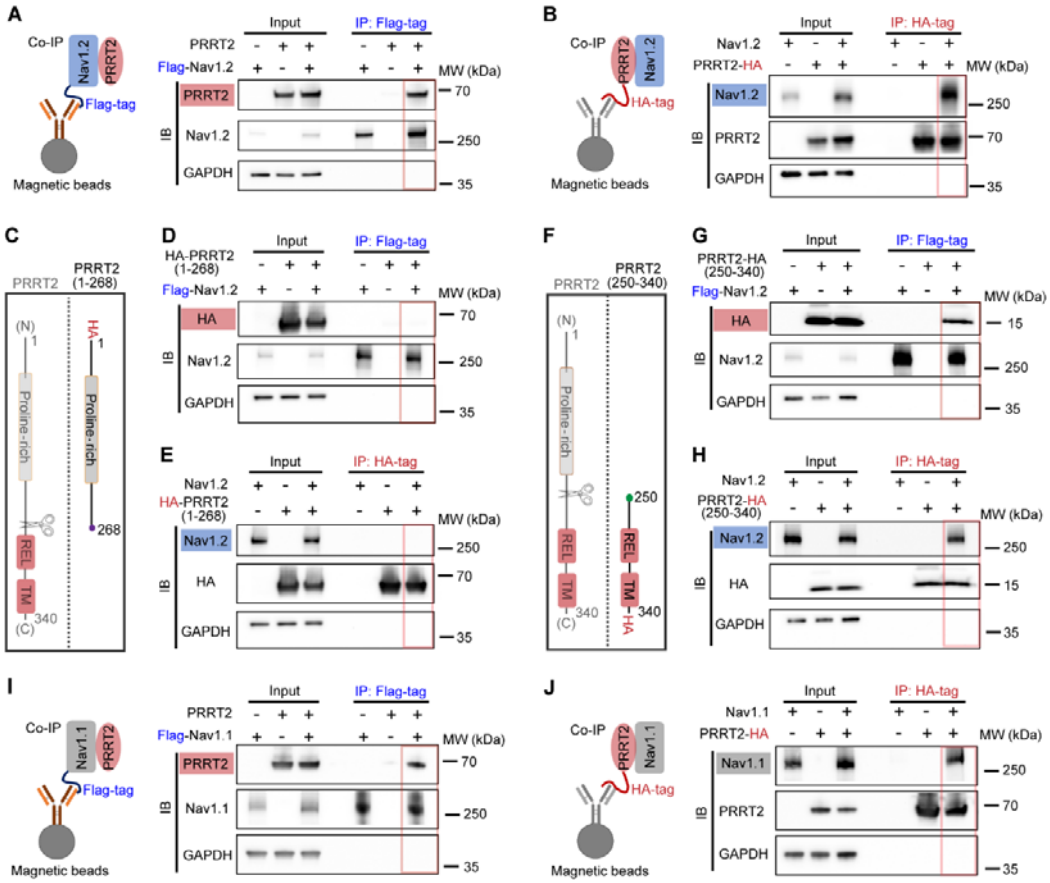

Figure 5 Intermolecular interaction between PRRT2 and Nav channels *in vitro*

(A and B) Schematic diagram showing the co-immunoprecipitation for detecting human PRRT2-Nav1.2 interaction. Flag-tagged Nav1.2 (+), HA-tagged PRRT2 (+) and empty (-) vectors were transfected in HEK293T cells as indicated. The cell lysates were immunoprecipitated with anti-Flag (A) or anti-HA (B) magnetic beads, the captured proteins were analyzed by SDS-PAGE and immunoblotting.

(C) Diagram for HA-tagged truncation of human PRRT2 (PRRT2(1–268)), in which the carboxyl terminus of PRRT2 was deleted. REL, re-entrant loop. TM, transmembrane domain.

(D and E) Co-immunoprecipitation assay for potential interaction between Nav1.2 and PRRT2(1–268). The proteins immunoprecipitated by anti-Flag (D) or anti-HA (E) magnetic beads were analyzed by immunoblotting. Note that HA-tagged PRRT2(1–268) was detected by anti-HA antibody in (D and E).

(F) Diagram for HA-tagged truncation of human PRRT2 (PRRT2(250–340)), in which the amino terminus of PRRT2 was deleted.

(G and H) Co-immunoprecipitation assay for potent interaction between Nav1.2 and PRRT2(250–340). The proteins immunoprecipitated by anti-Flag (G) or anti-HA (H) were analyzed by immunoblotting. Note that HA-tagged PRRT2(250–340) was detected by anti-HA antibody in (G and H).

(I and J) Co-immunoprecipitation assay for potential interaction between Nav1.1 and PRRT2. The proteins captured by anti-Flag (I) or anti-HA (J) magnetic beads were analyzed by immunoblotting. In (A, B, D, E, G, H, I and J), blots shown are representative of at least three independent co-immunoprecipitation experiments with similar results. Red rectangles indicate the immunoblotting of bait and potential prey proteins in co-immunoprecipitation. IB, immunoblot. IP, immunoprecipitation. MW, molecular weight.

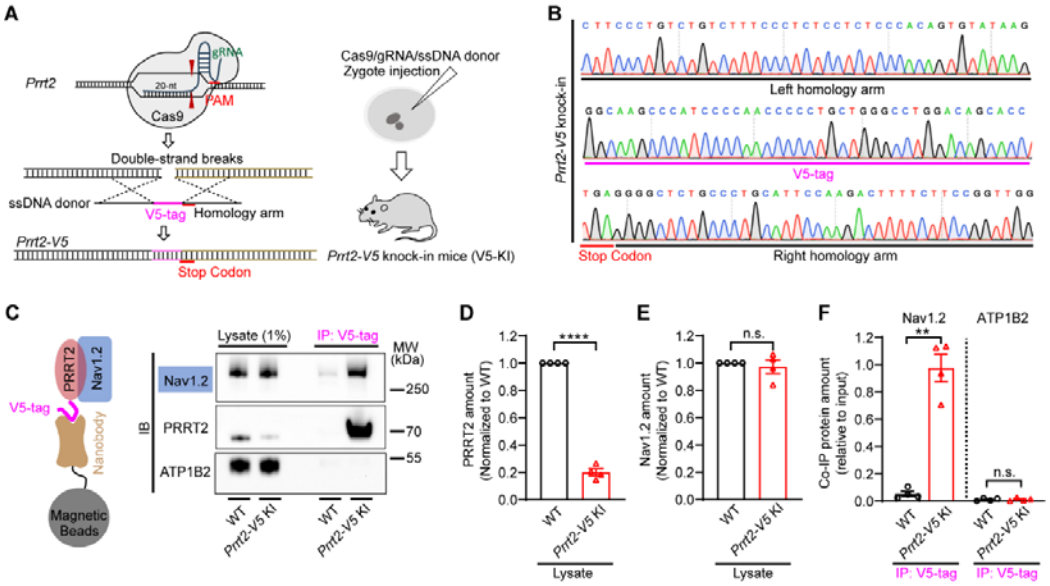

Figure 6 PRRT2 forms a molecular complex with Nav1.2 in the mouse brain

(A) Schematic showing the generation of *Prrt2-V5* knock-in (V5-KI) mice using Cas9 technology. V5-tag sequence was inserted precisely at the end of *Prrt2* gene. PAM, protospacer-adjacent motif (NGG). ssDNA, single-strand DNA.

(B) Sanger sequencing around sgRNA targeting site in *Prrt2-V5* knock-in mouse. The V5-tag, stop codon and homologous arms were denoted.

(C) Co-immunoprecipitation assay for potential interaction between Nav1.2 and PRRT2-V5 in the brain tissue. The proteins immunoprecipitated by anti-V5 nanobody were analyzed by immunoblotting. Blots shown are representative of four independent co-immunoprecipitation experiments. IB, immunoblot. IP, immunoprecipitation. MW, molecular weight. WT, wild-type. KI, knock-in.

(D-F) Quantification of the density of protein bands for PRRT2 (D) and Nav1.2 (E) in lysate, and for Nav1.2 and ATP1B2 in Co-immunoprecipitation experiments (F) (n = 4 mice for each group). Data were presented as mean ± s.e.m. In (D-F), two-tailed, paired Student's t-test was used for determining statistical significance. $^{**}P < 0.01$, $^{****}P < 0.0001$, n.s., not significant.

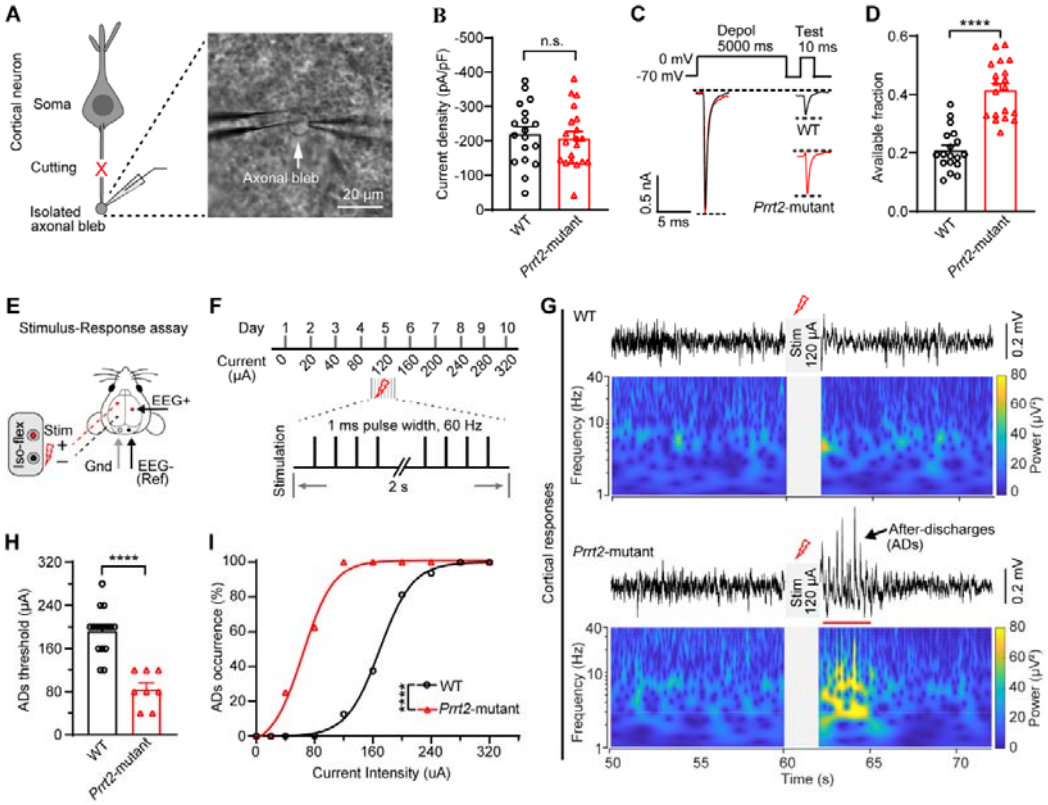

Figure 7 PRRT2 deficiency impairs the regulation of Nav channel slow inactivation and neuronal resilience in mice

(A) Schematic showing the isolated axonal bleb recording in cortical neuron (left) and the representative brightfield image for the axonal bleb in brain slice (right). The arrow indicates an axonal bled. Scale bar, 20 µm.

(B) Sodium current density recorded in isolated axonal blebs from wild-type (WT) and *Prrt2*-mutant mice (WT: *n* = 18 blebs from 7 mice, *Prrt2*-mutant: *n* = 20 blebs from 8 mice).

(C) Protocol for assessing Nav channel slow-inactivation (upper) and the representative traces of the sodium currents evoked by conditioning depolarization pulse and test pulses (bottom). Scale bar, 0.5 nA by 5 ms.

(D) Fraction of available Nav channels after 5-s depolarization (WT: *n* = 18 blebs from 7 mice, *Prrt2*-mutant: *n* = 19 blebs from 8 mice).

(E) Schematic illustration of the cortical electrostimulation and EEG recording in mice. Ref, reference electrode. Gnd, ground electrode. Stim, Stimulation.

(F) Illustration showing the experimental schedule and the stimulation parameters. Stimulation was delivered once daily with stepwise increases in current intensity.

(G) Representative traces and power of EEG signals in wild-type and *Prrt2*-mutant mice before and after 2-s cortical stimulation. After-discharges were indicated by the arrow and red line. Scale bar: 0.2 mV. Electrical stimulation (120 μA) was applied during 60–62 s period, where the stimulus-induced artifacts were removed prior to analysis.

(H) Threshold of electrical stimulation to induce after-discharges in WT and *Prrt2*-mutant mice (WT: n = 16 mice, *Prrt2*-mutant: n = 8 mice).

(I) Percentage of after-discharge occurrence in WT and *Prrt2*-mutant mice after electrical stimulation (WT: n = 16, *Prrt2*-mutant: n = 8). Data were presented as mean ± s.e.m. Two-tailed, unpaired Student's *t*-test was used in (B and D) and two-tailed, unpaired Mann-Whitney test was used in (H). In (I), the main effect of group was assessed using two-way ANOVAs. ****P < 0.0001, n.s., not significant.

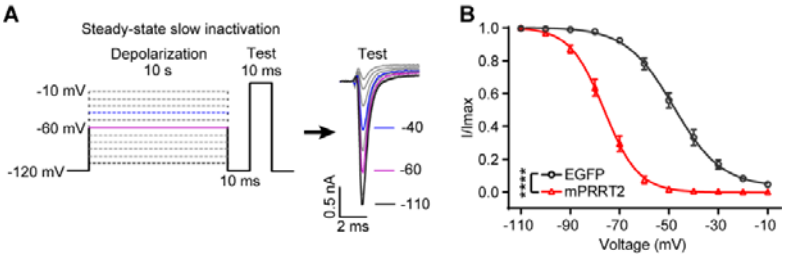

Figure 1-figure supplement 1. PRRT2 promotes steady-state slow inactivation

(A) Protocol of steady-state slow inactivation test (left) and representative traces of the sodium currents evoked by test pulses (right). The sodium currents gradually decreased as the voltage in conditioning steps increased. Scale bar, 0.5 nA by 2 ms.

(B and C) The effects of PRRT2 on voltage-dependent steady-state slow inactivation of Nav1.2 channels (B) (EGFP: *n* = 11 cells, mPRRT2: *n* = 13 cells). mPRRT2, mouse PRRT2. Data were presented as mean ± s.e.m. Two-way ANOVAs were used in (B) to determine the statistical significance of main effects of group. ****$P < 0.0001$.

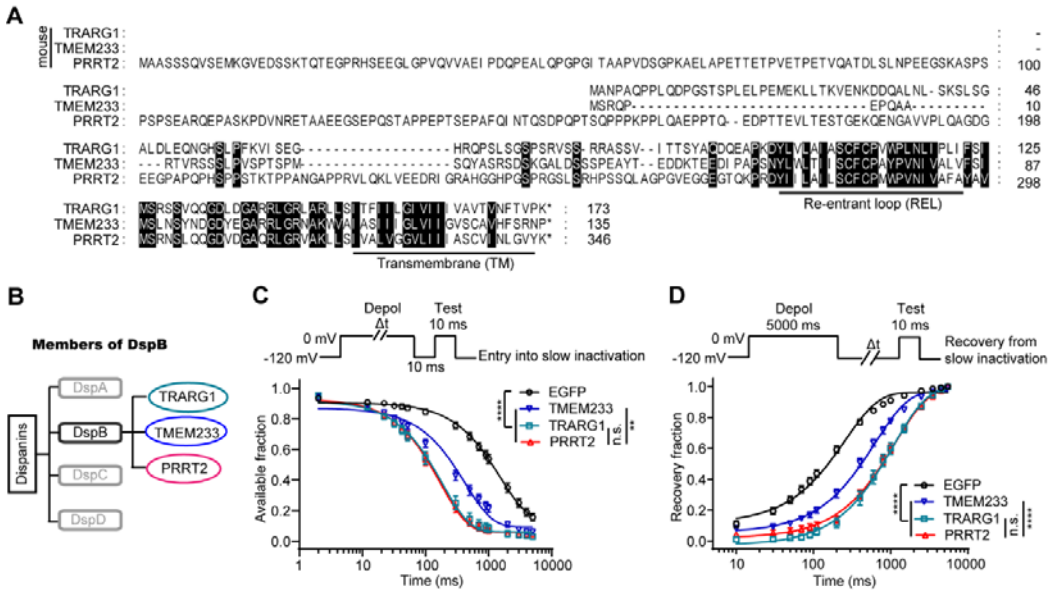

Figure 3-figure supplement 2. Paralogs of PRRT2 regulate Nav channel slow inactivation

(A) Sequence alignment of mouse TRARG1, TMEM233 and PRRT2 proteins. Conserved amino acids are highlighted and the transmembrane domains in carboxyl terminus of these proteins are underlined. REL, re-entrant loop. TM, transmembrane domain.

(B) Schematic showing the phylogenetic relationship between members of Dispanin subfamily B (DspB).

(C) The effects of members of DspB on the entry of Nav1.2 channels into slow inactivation (EGFP: *n* = 13 cells, TRARG1: *n* = 17 cells, TMEM233: *n* = 13 cells, PRRT2: *n* = 13 cells).

(D) The effects of members of DspB on the recovery of Nav1.2 channels from slow-inactivated states induced by 5-s depolarization (EGFP: *n* = 10 cells, TRARG1: *n* = 14 cells, TMEM233: *n* = 12 cells, PRRT2: *n* = 12 cells).

Data were presented as mean ± s.e.m. The main effect of group was assessed using two-way ANOVAs (C and D). ***P* < 0.01, *****P* < 0.0001, n.s., not significant.

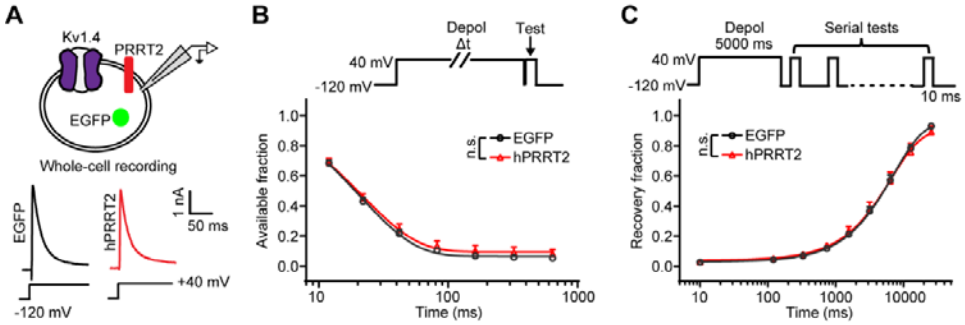

Figure 4-figure supplement 3. Absence of effect of PRRT2 on Kv1.4 channel inactivation

(A) Illustration showing the whole-cell voltage-clamp recording in Kv1.4 stably expressing HEK293T cells (upper) and representative traces of potassium currents evoked by a depolarization at 40 mV (bottom). Scale bar, 1 nA by 50 ms.

(B) The effects of human PRRT2 on the entry of Kv1.4 channels into inactivated state (EGFP: *n* = 9 cells, hPRRT2: *n* = 8 cells).

(C) The effects of human PRRT2 on the recovery of Kv1.4 channels from inactivated states induced by 5-s depolarization (EGFP: *n* = 8 cells; hPRRT2: *n* = 7 cells).

Data were presented as mean ± s.e.m. The main effect of group was assessed using two-way ANOVAs (B and C). n.s., not significant.

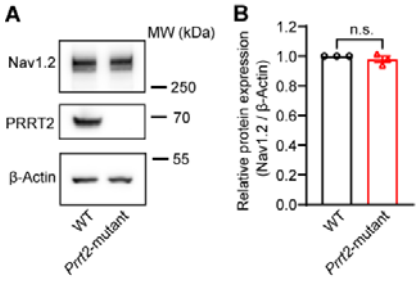

Figure 7-figure supplement 4. Protein levels of Nav1.2 are unchanged in brain tissue from *Prrt2*-mutant mice

(A and B) Immunoblots (A) and quantifications (B) of Nav1.2 proteins in brain tissue of wild-type (WT) and *Prrt2*-mutant mice (n = 3 mice). Data were presented as mean ± s.e.m. Two-tailed, paired Student's t-test was used in (B) to determine the statistical significance. n.s., not significant.